



Kämäri, M., Tattari, S., Lotsari, E., Koskiaho, J., & Lloyd, C. E. M. (2018). High-frequency monitoring reveals seasonal and event-scale water quality variation in a temporally frozen river. *Journal of Hydrology*, 564, 619-639. <https://doi.org/10.1016/j.jhydrol.2018.07.037>

Peer reviewed version

License (if available):  
CC BY-NC-ND

Link to published version (if available):  
[10.1016/j.jhydrol.2018.07.037](https://doi.org/10.1016/j.jhydrol.2018.07.037)

[Link to publication record in Explore Bristol Research](#)  
PDF-document

This is the author accepted manuscript (AAM). The final published version (version of record) is available online via Elsevier at <https://www.sciencedirect.com/science/article/pii/S0022169418305420> . Please refer to any applicable terms of use of the publisher.

## University of Bristol - Explore Bristol Research

### General rights

This document is made available in accordance with publisher policies. Please cite only the published version using the reference above. Full terms of use are available:  
<http://www.bristol.ac.uk/red/research-policy/pure/user-guides/ebr-terms/>

# Accepted Manuscript

Research papers

High-frequency monitoring reveals seasonal and event-scale water quality variation in a temporally frozen river

M. Kämäri, S. Tattari, E. Lotsari, J. Koskiahho, C.E.M. Lloyd

PII: S0022-1694(18)30542-0

DOI: <https://doi.org/10.1016/j.jhydrol.2018.07.037>

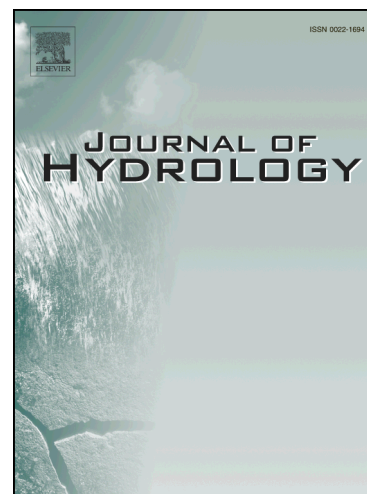
Reference: HYDROL 22969

To appear in: *Journal of Hydrology*

Received Date: 27 June 2017

Revised Date: 20 June 2018

Accepted Date: 14 July 2018



Please cite this article as: Kämäri, M., Tattari, S., Lotsari, E., Koskiahho, J., Lloyd, C.E.M., High-frequency monitoring reveals seasonal and event-scale water quality variation in a temporally frozen river, *Journal of Hydrology* (2018), doi: <https://doi.org/10.1016/j.jhydrol.2018.07.037>

This is a PDF file of an unedited manuscript that has been accepted for publication. As a service to our customers we are providing this early version of the manuscript. The manuscript will undergo copyediting, typesetting, and review of the resulting proof before it is published in its final form. Please note that during the production process errors may be discovered which could affect the content, and all legal disclaimers that apply to the journal pertain.

# High-frequency monitoring reveals seasonal and event-scale water quality variation in a temporally frozen river

M. Kämäri<sup>a,b</sup>, S. Tattari<sup>b</sup>, E. Lotsari<sup>a,c</sup>, J. Koskiaho<sup>b</sup>, C.E.M. Lloyd<sup>d</sup>

<sup>a</sup>Department of Geographical and Historical Studies, University of Eastern Finland, Yliopistokatu 2, P.O. Box 111, 80101 Joensuu, Finland

<sup>b</sup>Finnish Environment Institute, SYKE, Mechelininkatu 34a, 00251 Helsinki, Finland

<sup>c</sup>Department of Geography and Geology, University of Turku, 20014 Turun yliopisto, Turku, Finland

<sup>d</sup>School of Chemistry, University of Bristol, Cantock's Close, Bristol BS8 1TS, UK

**Keywords:** snowmelt, in-situ monitoring, turbidity, nitrate-nitrogen, dissolved organic carbon, hysteresis

## Abstract

Potential influences of climate change on water quality, riverine suspended sediments, nitrogen and organic matter loads in temporally frozen rivers, which have ice-covered flow and snow-affected basins, are poorly understood. However, before being able to understand potential future changes, the impact of ice and snow needs to be investigated more thoroughly for years which were hydrologically different. We investigated seasonal and event scale concentration-discharge (C-Q) dynamics of total suspended solids/turbidity, nitrate-N ( $\text{NO}_3\text{-N}$ ) and chemical oxygen demand (COD), which is indicative of the amount of organic matter in river water. In particular, the influence of ice cover, contrasting spring thaw, and soil frost conditions on intra-annual fluxes and the C-Q response of the three solutes are detected based on over four years of hourly data. Seasonally flow-weighted suspended solids and  $\text{NO}_3\text{-N}$  concentrations were at their highest in either the autumn or spring thaw, but COD concentrations were the highest each year in autumn.  $\text{NO}_3\text{-N}$  and COD levels typically decreased during winter. The ice-covered river water was less turbid compared to open-channel water at an equivalent river discharge likely due to in-stream factors. Storms during the freshet period introduced flushing of organic matter and suspended solids. The ratio of organic matter yield to water yield was similar each freshet and was independent of the amount of precipitation as snow or soil frost status. The freshet  $\text{NO}_3\text{-N}$  yield per water yield was higher during the years with a thick snowpack and the consequent thawed soil compared to a year with soil frost and minor snowpack. 91 storm events studied revealed differences and similarities in storm

dynamics in between the three variables. Anti-clockwise hysteresis was most common for the variables, with turbidity peaking faster than the COD or  $\text{NO}_3\text{-N}$  concentration in most of the storms. Snowmelt storms showed highly variable C-Q responses inbetween the variables. However, spring thaw-related COD concentration peaks abated more slowly compared to turbidity or  $\text{NO}_3\text{-N}$ .  $\text{NO}_3\text{-N}$  showed a strong dilution pattern during several autumn storms during an extremely wet year, indicating limited N sources for flushing from the catchment. As a result, the flow-weighted mean  $\text{NO}_3\text{-N}$  concentration was not the largest during the year of largest water yield instead which was true for suspended solids and COD. We found no evidence that warmer winters with precipitation as rain instead of snow would increase suspended sediment, organic matter and  $\text{NO}_3\text{-N}$  load at entire winter-spring season or annual timescales.

## 1. Introduction

Climate predictions indicate warming winters in parts of the cold regions in the Northern Hemisphere (Luterbacher et al., 2004; Ruosteenoja et al., 2007, 2016) where atmospheric circulation patterns strongly influence air temperatures as well as freshwater ice durations (Prowse et al., 2011). River-ice cover periods have decreased (Magnuson et al., 2000), which may in turn enhance winter time river bed erosion and riverine transportation of suspended sediments downstream (Kämäri et al., 2015). Earlier snow clearance is a trend at the Eurasian scale (Takala et al., 2009) and snow cover duration has decreased at Northern Hemisphere (Brown and Mote, 2009; Brown and Robinson 2011). Climate change may overall flatten the hydrograph by decreasing the magnitude of flashy spring snowmelt discharges due to reducing snow accumulation (Prowse et al., 2006; Veijalainen et al., 2010). In addition, changes in soil frost, freeze-thaw cycles and snowmelt timing are expected, which will impact on riverine biogeochemistry and the amount and timing of nutrient export (Su et al., 2011). In the mid-latitude areas of the Northern Hemisphere, long-term precipitation increase is evident (IPCC, 2014). Regional increases of winter and spring precipitation totals have been projected for the future (Olsson et al., 2015; Ruosteenoja et al., 2016), which enhances particle bound nutrient losses from catchments into streams, since agricultural

fields are particularly vulnerable to leaching during dormant periods (Puustinen et al., 2007; Rosberg and Arheimer, 2007). Also, frequent rainfall on frozen soils can increase surface erosion (Su et al., 2011). However, seasonal and annual variations in riverine suspended sediments, nitrogen and organic matter loads in temporally frozen rivers, which have ice-covered flow and snow-affected basins during winter months, are poorly understood at present. Therefore spatio-temporal dynamics need to be investigated in more detail before being able to make more precise future predictions.

Snowpack and soil frost status, are some of the many factors which influence nutrient cycling as well as sediment net erosion rates, which are again reflected in river water quality. Microbial activity in consistently snow-covered soil may provide a buffer thereby limiting the export of  $\text{NO}_3\text{-N}$  into rivers during snowmelt, but the process is highly sensitive to changes in the snowpack regime (Brooks et al., 1998; Shibata et al., 2013). Furthermore, the effect of variations in snow cover extent and depth on dissolved organic carbon (DOC) dynamics is uncertain (Brooks et al., 2011). Lack of snow and related enhanced soil frost has been shown to increase DOC in forest soils, leading to increased concentrations of DOC in the adjacent streams (Haei et al., 2010). However, Finlay et al. (2006) reported that the proportion of annual DOC flux in snowmelt is higher than for water in an arctic river. Changes in snow cover, temperature and precipitation have potentially profound impacts on the soil and surface water hydrology during winter and spring. There are also highly unclear net effects on annual and longer-term patterns of N or DOC cycling and riverine fluxes (Brooks et al., 2011; Haei et al., 2010), as freshet period and snowpack profoundly contribute to the annual DOC (Holmes et al., 2008), nitrogen (N) (Brooks and Williams, 1999) and suspended sediment yield (Kämäri et al., 2015; McDonald and Lamoureux, 2009). The influence of the frozen season and spring thaw on nutrient or DOC concentrations and fluxes has been studied in alpine and Arctic rivers (Boyer et al., 1997; Guo et al., 2012), forested field sites (Haei et al., 2010; Pellerin et al., 2012; Sebestyen et al., 2008) and in a laboratory (Campbell et al., 2014). However, the impact on sediment and nutrient cycle, as snow-dominated winters change to rain-dominated ones, has not yet been widely studied in temperate rivers, which will experience the future reduction in frozen periods the fastest.

85 High-frequency water quality monitoring allows determination of timing and quantification  
86 of event scale material fluxes and enhance understanding of the key mechanisms behind the observed  
87 riverine water quality variations and of potential future behaviours (Blaen et al., 2016). Therefore, multi-  
88 year, hourly water quality and discharge observations allow the determination of not only annual and  
89 seasonal loadings (Cassidy and Jordan, 2011; O'Flynn et al., 2010; Worrall et al., 2013), but also short-  
90 term concentration-discharge relationships (C-Q) more robustly than traditional grab sampling. Diurnal  
91 fluctuations of nutrient or dissolved organic matter (DOM) concentrations due to varying biogeochemical  
92 mechanisms (Spencer et al., 2007) driven by water temperature (Scholefield et al., 2005) snowmelt pulses  
93 (Pellerin et al., 2012) or photic removal (Worrall et al., 2015), may influence load estimates (Jones et al.,  
94 2012) yet can only be captured with high frequency monitoring. Riverine load estimates determined on  
95 the basis of lower frequency water sampling are often different from those made by high-frequency  
96 sensors (Lloyd et al., 2016a; Jones et al., 2012; Williams et al., 2015).

97 Recently, the number of studies using high-frequency riverine nutrient monitoring has  
98 increased (e.g. Bende-Michl et al., 2013; Bieroza and Heathwaite, 2015; Lloyd et al., 2016b; Pellerin et  
99 al., 2012; Koskiahio et al., 2015; Kotamäki et al., 2009; Valkama and Ruth, 2017). Many of these studies  
100 have analysed solute hysteresis, flushing or dilution patterns describing the C-Q responses

101 of  $\text{NO}_3\text{-N}$  (Ockenden et al., 2016; Outram et al., 2014), DOC (Strohmeier et al., 2013;  
102 Worrall et al., 2015) as well as turbidity or suspended sediments (Cerro et al., 2014; Valkama and Ruth  
103 2017). Also studies have shown large variations in nutrient transport related to discharge events of  
104 varying magnitude and order of occurrence (e.g. Lloyd et al., 2016c). There is currently a lack of event  
105 based C-Q studies from cold regions, from mixed land-use catchments as well as studies covering the  
106 entire annual hydrological cycle over several years (Table 1). Only few studies have yet concurrently  
107 examined the C-Q response of three water quality variables in connection with frozen and spring thaw  
108 periods (Table 1) to determination of how solute C-Q response timing and magnitude vary between  
109 substances and seasons.

Turbidity is the most common variable measured with in-situ optical sensors (Ockenden et al., 2016). If the relationships between turbidity and total suspended solids (TSS) ( $\text{mg L}^{-1}$ ) concentration and between turbidity and total phosphorus (TP) concentrations are significant, turbidity can be used as a surrogate for TSS and/or TP concentrations (Horsburgh et al., 2010; Jones et al., 2011, 2012; Tananaev and Debolskiy, 2014; Valkama and Ruth, 2017). Lloyd et al. (2016b) have proposed improvements to the analysis of hysteresis loops and believe it could become a standardised analytical technique in water quality research. Therefore, this method needs to be tested for a range of river sizes across the full spectrum of hydrological conditions.

Therefore, we aim to determine the impacts of hydro-climatic variation, e.g. discharge ( $Q$ ) ( $\text{m}^3 \text{s}^{-1}$ ), river ice, precipitation and snow water equivalent (SWE) (mm) on seasonal and event scale water quality and loadings in a temporally ice-covered river. The detailed objectives are:

- (i) to describe interannual and seasonal patterns in concentrations and loading of turbidity,  $\text{NO}_3\text{-N}$  and chemical oxygen demand (COD) ( $\text{mg L}^{-1}$ ), which is used as surrogate for DOC, including the ice-coved flow season;
- (ii) to quantify and compare event scale concentration-discharge patterns and loading of the three in-situ hourly monitored parameters during storm discharge events, including snowmelt;

To address these objectives, high-frequency, i.e., hourly discharge and water quality data were collected based on in-situ spectrophotometer measurements from the boreal Vantaa River in Southern Finland during a period of circa four years (2010–2014). We examined the C-Q relationship of the above-mentioned three river water quality variables during the frozen period and snowmelt, which provides novel insights to solute transportation in cold environment mixed land-use catchments. Contextual hydroclimatic data was collected from the river and surrounding watershed during the study period to help evaluate the relationships between their drivers and variability in water quality parameters.

<Table 1 here please>

136

## 137 2. Study site

138

139 The 101-km-long Vantaa River in southern Finland drains a 1680 km<sup>2</sup> watershed and flows into the Baltic  
 140 Sea (Fig. 1). The climate is characteristic of the boreal zone, with the monthly mean temperature varying  
 141 from -6.3°C in February to 17.1 °C in July (1981–2010) (Pirinen et al., 2012) . The average precipitation  
 142 is 660 mm y<sup>-1</sup>. The atmospheric deposition of NO<sub>3</sub>-N is 1.6 kg ha<sup>-1</sup> y<sup>-1</sup> (2000–2011) (Palviainen et al.,  
 143 2015). The mean surface gradient is 1.7 m km<sup>-1</sup>. The elevation ranges between 0 and 150 m a.s.l., and the  
 144 highest parts of the basin are in the North. Reliefs and moraines are present in the northern part of the  
 145 catchment, mostly covered by forest. Agricultural land and clay soils are predominant in the southern part  
 146 of the catchment, which is flat or slightly hilly. Agricultural (crops and grass ley) areas (23%) and forests  
 147 (57%) including peatland (0.5%) are the dominant land uses (Corine 2012 land use classification).  
 148 Therefore, the catchment can be categorised as mixed land use. Due to the small lake percentage (2%)  
 149 (Räike et al., 2012), the concentration and export of organic matter and N in the river are not largely  
 150 influenced by lake retention (Mattsson et al., 2015). A total of 18% of the basin is under urban land cover.  
 151 The basin soils are largely clay (40%) and moraine/sand (40%). At the outlet of the basin, the average  
 152 (1983–2013) Q is 11 m<sup>3</sup> s<sup>-1</sup> and ranges between 1 and 300 m<sup>3</sup> s<sup>-1</sup> (SYKE, 2017). The width of the river at  
 153 the high-frequency monitoring site 1 (see Fig. 1) is 37 m. Four municipal waste water treatment plants  
 154 within the catchment treat effluent waters totaling 170 000 person equivalents. Less than 8% of the DOC  
 155 originates from point sources (Räike et al., 2012).

156

157 <Figure 1 here please>

158

159 The long-term median COD concentration (COD<sub>Mn</sub>) of the Vantaa River basin is 14 mg L<sup>-1</sup>. COD (n =  
 160 465) correlates significantly with DOC (n = 452), as Pearson's correlation coefficient is 0.8, *p*<0.001  
 161 (Räike et al., 2012), thus COD may be used as a surrogate of DOC in this basin. COD can be used also as



a rough estimate of total organic carbon (TOC) ( $\text{mg L}^{-1}$ ) in aquatic ecosystems (Kortelainen, 1993). Typically, more than 90% of TOC is in dissolved form in Finnish rivers (Mattsson et al., 2005). The proportion of organic soil in the drainage basin is the major factor influencing the DOC concentrations in runoff and may mask possible effects of land use on DOC concentrations (Autio et al., 2016). The TOC export correlates positively with the amount of peatland while total organic N and  $\text{NO}_3\text{-N}$  export increases with the increasing percentage of agricultural land in Finnish basins (Mattsson et al., 2005). The amount of peatland in the study catchment is less than average for Finland (Räike et al., 2012).

### 3. Material and methods

#### 3.1 River discharge, river-ice snow and precipitation data

Discharge was determined based on a weir specific stage-discharge curve. Water level was measured with a pressure sensor, Keller AG, with  $\pm 1$  mm resolution at site 1. Manual water level measurements were made (see Figure S1 in the supplementary material) to ensure the quality of the pressure sensor data. Typical storm hydrographs display sharp rising limbs, and the return to baseline lasted typically a month or more. The mean  $Q$  was  $11 \text{ m}^3 \text{ s}^{-1}$  with low discharge during mid-winter (Feb.  $Q_{\text{mean}} = 5.4 \text{ m}^3 \text{ s}^{-1}$ ) and the growing season (June-Aug.  $Q_{\text{mean}} = 2.7 \text{ m}^3 \text{ s}^{-1}$ ).

River ice thicknesses were measured twice a month at two sites (sites 2 and 3), which were located 8.6 and 4.2 km upstream from the river mouth (Fig. 1). The ice thicknesses are shown in the Supplementary material (Fig. S1) and were collected from the data base of the Finnish Environment Institute. The exact dates of the formation of the river ice or ice breakup were not monitored, but ice-cover periods when the river was definitely frozen were estimated by Kämäri et al. (2016) (see Table 2) based on water and air temperatures, in addition to measured river-ice thickness (Fig. S1). The SWE observations were derived from the three most representative sites from the national SWE monitoring network (SYKE, 2017). The snow courses were sampled twice a month and the mean value of the sites were calculated. The areal SWE maps summarise the snowpack variation during February-April 2011–

2014 based on the nationwide observation network from over 140 monitoring sites (see Figure S2). Furthermore, the areal average snow depth (cm) (Table 2) is based on manual sampling at the weather stations and the data are provided by the Finnish Meteorological Institute (FMI). Daily precipitation and daily mean air temperatures are from Helsinki Airport located approximately 5 km distance of Site 1 (FMI, open data portal). Soil frost data at two measurement sites in Southern Finland are provided and compared to long-term average values in the Supplementary Material (Table S1).

<Table 2 here please >

## 3.2 In-situ water quality monitoring approach

### 3.2.1 Specifications of the spectrophotometer

An ultraviolet-visible (UV/vis) spectrophotometer (scanco spectrophotometer, scanco Messtechnik GmbH, Austria) (van den Broeke et al., 2006) was used to monitor in-situ light absorbance in the wavelength region 200–735 nm between Oct 2010 and Dec 2014. The DOC measurement started first Dec 3, 2010. The sensor was installed one metre above the river bed to measure ‘raw’ turbidity, NO<sub>3</sub>-N and DOC values at site 1 at hourly intervals (Fig. 1). Water samples (n = 6) were taken along the cross-section of the in-situ sensor. The results confirm that the location of the sensor was representative and did not cause any noticeable bias to the measured concentrations or load estimates, since the grab sample concentrations did not fluctuate along the cross-section.

An optical path length of 5 mm was used, since a larger path length would have resulted in interference due to turbidity. Automatic compressed air cleaning of the optical lenses and 50 seconds of heating of the probe took place prior to each measurement. Manual cleaning of the sensor was also carried out every 2 to 8 weeks. Under optimal conditions, the accuracy of ‘raw’ turbidity, NO<sub>3</sub>-N and DOC in-situ measurements is about  $\pm 3$  FTU (Formazin Turbidity Units),  $\pm 0.2$  mg L<sup>-1</sup> and  $\pm 0.5$  mg L<sup>-1</sup>,

respectively (Kiirikki, 2018). Post-measurement data processing revealed that the high turbidity observed (approximately 300–450 FTU) influenced  $\text{NO}_3\text{-N}$  measurements but not DOC measurements, due to the different spectral detection range. Thus,  $\text{NO}_3\text{-N}$  records during the highest turbidity period (20–21/10/2011) were flagged as erroneous and deleted from the analysis. There was a period from December 2012 – January 2013 when the UV/vis sensor data was not retrieved, due to human error. That data gap and an additional small number short data gaps, e.g. due to maintenance, were linearly interpolated.

### 3.2.2 Calibration of the spectrophotometer

Turbidity,  $\text{NO}_3\text{-N}$ , and COD grab samples were collected from site 1 and analysed in an accredited laboratory for the purpose of determining linear calibration equations (Eq. 1) for the in-situ sensor data. The sum of  $\text{NO}_3\text{-N}$  and nitrite ( $\text{NO}_2\text{-N}$ ) was determined with a method based on standard EN ISO 13395. In this method  $\text{NO}_3\text{-N}$  is reduced to  $\text{NO}_2\text{-N}$  by a copper-cadmium reductor column.  $\text{NO}_2\text{-N}$  is determined by diazotizing with sulfanilamide and coupling with N-(1-naphthyl)-ethylenediamine to form a reddish-purple azo dye that is measured at a wavelength of 520 nm. The analysis method for COD is based on Finnish Standard SFS 3036. A known amount of potassium permanganate is added to a sample which has been acidified with sulphuric acid. The sample is then heated for 20 minutes in boiling water. Oxidisable material in the sample reduces part of the permanganate. The unreduced portion of permanganate is determined iodometrically by titrating with sodium thiosulphate. The consumption of permanganate is used for the calculation of COD value. Water grab sampling was temporally well distributed, since the collected samples represented the observed Q range and variation (Fig. 2).

<Figure 2 here please>

The in-situ raw values for turbidity,  $\text{NO}_3\text{-N}$  and DOC were converted into turbidity and TSS concentrations,  $\text{NO}_3\text{-N}$  concentrations and COD concentrations respectively according to Eq. 1:

$$(1) c = B \cdot x + a$$

where  $c$  is the calibrated in-situ sensor value,  $x$  is the primary in-situ value,  $B$  is slope and  $a$  is intercept retrieved from least squares regression. COD is a measure of the total amount of oxygen required to oxidise all organic detritus into carbon dioxide and water, and can be used to indicate variations in the amount of soluble and particulate organic and inorganic matter in the river.

The site-specific calibration equations and standard error of the estimates ( $S_{\text{est}}$ ) – i.e. the estimates of the average error of the regression models – are provided in Table 3. The residuals were approximately normally distributed; thus, the uncertainty related to the in-situ data can be estimated from the standard error of the estimates. Statistically, about 2/3 of the in-situ sensor calibrated values should be and were in the range  $\pm S_{\text{est}}$  and 95% in the range  $\pm 2S_{\text{est}}$  of laboratory measured values for each determinant. The coefficients of determination for the in-situ measurement model equations were between 0.83 and 0.93 (Table 3).

<Table 3 here please>

### 3.2.3 Validation of the spectrophotometer data

The calibrated in-situ hourly data were verified against grab sample values from the national water quality monitoring (site 2) situated 3.8 km downstream from the in-situ monitoring site (site 1). At site 2 manual water samples were collected on average 10 times per year and turbidity,  $\text{NO}_3\text{-N}$  and COD were analysed in a manner similar to the grab samples from site 1. The difference in catchment size between sites 1 and 2 was only 1% and, thus water quality is expected to be quite similar. The performance of the in-situ sensor was visually (Fig. 3) and statistically (Table 4) analysed against sampled values from sites 1 and 2. The sensor captured several turbidity,  $\text{NO}_3\text{-N}$  and COD peaks that were sampled from site 2, thus

indicating that the calibration of the sensor was successful. The standard error of the in-situ  $\text{NO}_3\text{-N}$  estimates were the same between the two sites, and only slightly higher for turbidity and COD in site 2. The percentage of mean errors between concentrations calculated based on laboratory analysis and based on in-situ sensors measurements were 12–20% at site 1 and 13–37% at site 2. The median percentage error was smaller at both sites (Table 4). The percentage error is sensitive to relatively small absolute errors during low concentrations. The visual check of in-situ sensor concentrations against laboratory samples reveal, that the in-situ sensor excellently captured the variation of all concentrations (Fig. 3).

<Table 4 here please>

<Figure 3 here please>

### 3.3 Seasonal and event scale analyses

#### 3.3.1 Seasonal water quality and loads

The flow-weighted mean concentrations were calculated by dividing the total load over the estimation time period by the total streamflow. The flow-weighted mean concentrations were determined on an annual and monthly basis for the purpose of revealing potential differences in solute flushing at different temporal scales. Furthermore, the daily average solute concentrations were calculated and compared between ice-covered and open-water conditions at equivalent discharges, in order to detect potential ice-cover influences on suspended solids transport and solute concentrations.

Distinct winter temperature, soil frost, snow accumulation and melt pattern occurred between the four years study period. Solute fluxes as well as flow-weighted mean concentrations from Nov. to May, i.e. entire winter-spring, periods were calculated. The effect of very different ambient spring thaw conditions on solute fluxes was separately investigated by calculating cumulative solute and water yields during 60 days spring freshet (starting each year from the estimated ice clearance date, Table 2). The sediment and

nutrient yields against water yield were evaluated to detect potential differences of solute behaviour due to the varying length of frost season, magnitude of SWE, snowmelt and soil frost conditions.

### 3.3.2 Event-scale concentration-discharge response analyses

Altogether 91 discharge events, i.e. storms, were identified. The storms were defined to start at the point when the discharge started to rise by at least 20% of the initial discharge. The storms lasted as long as the discharge or the concentration of the water quality parameter took to return to the initial level. In the case of subsequent storms when the water quality or discharge did not return into the starting level, the storms were determined to end at the point when the next peak started to rise. Within the context of this paper, hysteresis is defined as a nonlinear relationship between discharge and solute concentration. Potential sources and pathways of the three water quality parameters seasonally and during snowmelt were analysed based on the observed C-Q patterns. A hysteresis index (H index / HI) was calculated for each storm, based on the difference in chemical concentration between the rising and falling limb of the storm hydrograph (Lloyd et al., 2016b):

$$(4) HI = \frac{1}{n} \sum HI_{Qi} = \frac{1}{n} \sum (C_{RL_{Qi}} - C_{FL_{Qi}})$$

where  $C_{RL_{Qi}}$  is the normalised concentration of the water quality parameter or turbidity at a given point  $i$  of  $Q$  on the rising limb of the hydrograph and  $C_{FL_{Qi}}$  is the value on the falling limb.  $n$  is the number of sections where the  $HI_{Qi}$  is calculated. In this study,  $HI_{Qi}$  was calculated at 5% increments of discharge between the starting  $Q$  and  $Q_{peak}$  of the storm. A 5% increment was selected based on earlier research, as it is likely that addition of more sections would not have altered the results significantly (Lloyd et al., 2016b). The mean overall  $HI_{Qi}$  values were used as the final HI value for each storm. The index provides values between -1 and 1, the larger the value the ‘fatter’ the loop and the stronger the hysteresis. The sign of the index illustrates the direction of the loop. Positive values indicate a clockwise loop where the

concentration peak occurs before the peak in the discharge event. Negative HI values present anti-clockwise loops, where the concentration peak lags behind the discharge peak. HI being close to zero (approximately  $-0.1 < HI < 0.1$ ) indicates three options. Firstly, a synchronised C-Q response during the rising and falling limbs of the storm, or secondly a figure-of-eight configuration, which combines clockwise and anti-clockwise loops. The third option is an unclear C-Q response, which may occur, especially during small discharge peaks, when there is no clear change in concentration.

The semi-quantitative descriptor  $\Delta C$  (flushing index) summarises concentration changes during the rising limb of storms (Butturini et al., 2008):

$$(5) \Delta C = \begin{cases} \frac{C_s - C_b}{C_s} 100, & \text{if } C_s > C_b \\ \frac{C_s - C_b}{C_b} 100, & \text{if } C_s < C_b \end{cases}$$

where  $C_b$  and  $C_s$  are concentrations at the initial discharge of the storm and during the peak of the discharge hydrograph, respectively.  $\Delta C$  can range from  $-100$  to  $100$ . Positive values indicate flushing of substances. Negative values indicate dilution during the rising limb of the flow hydrograph. Based on HI and  $\Delta C$ , the C-Q response distribution of a solute was visually presented in a unity plane (Butturini et al., 2008). Viewed in this way the storm responses of the solutes are divided according to hysteresis type and patterns of solute flushing or dilution.

Additionally, in order to compare the C-Q response of the monitored variables, the maximum Q ( $Q_{\text{peak}}$ ),  $Q_{\text{range}}$ , storm duration, mean solute concentration, solute concentration range and load, as well as the lag time between concentration peaks and the  $Q_{\text{peak}}$ s were calculated for each storm. The solute range is the difference between the solute minimum and maximum concentrations during a storm event. Spearman's correlation and the nonparametric Mann-Whitney U test in the IBM SPSS Statistics 23 software were employed to detect potential seasonality in the C-Q relationship and similarities in the C-Q response of the three solutes.

## 4. Results

### 4.1 Interannual and seasonal water quality and loads

#### 4.1.1 Variation in water quality

The flow-weighted mean concentrations of TSS and COD as well as Q were the largest during Nov. 2011–Nov. 2012 (Table 5). However, the flow-weighted mean concentration of  $\text{NO}_3\text{-N}$  was not particularly high during the extremely wet water year of 2011–2012. The monthly flow-weighted concentrations of TSS and  $\text{NO}_3\text{-N}$  were the highest either during the autumn or the spring thaw, however COD concentrations were the largest each year in the autumn (Fig. 4). The monthly mean  $\text{NO}_3\text{-N}$  concentrations were the lowest in the summer. The suspended solids concentrations were higher during Jun. – Aug. 2014 ( $38 \text{ mg L}^{-1}$ ) compared with the other three summers ( $19 - 30 \text{ mg L}^{-1}$ ) (Fig. 4).

<Table 5 here please>

<Figure 4. here please >

The river water was less turbid when ice-covered compared with the summer or autumn open-channel conditions at equivalent discharges (Fig. 5). The trend lines indicated that the daily average turbidity in the summer was approximately 100% and in the autumn 70% larger than when the river was ice-covered at the equivalent discharge, whereas COD behaved similarly during ice-covered conditions and during the summer (Fig. 5). During the autumn the COD concentrations were typically the largest compared to other seasons (Figs. 4 and 5). There was a negative relationship between Q and  $\text{NO}_3\text{-N}$  when the river was ice-covered, whereas the relationship was positive during autumn and summer (Fig. 5).

<Figure 5 here please>



#### 4.1.2 Variation in TSS, NO<sub>3</sub>-N and organic matter loads

The annual loadings were the largest during the hydrological year with the largest  $Q_{\text{mean}}$  (Table 5.). The effect of precipitation as rain instead of snow on seasonal loadings was investigated. The frost winters of 2011 and 2013 were long, the ice cover existed in the river for over 100 days, and the snowpack was still significant in mid-April. The winters 2012 and 2014 were both short in terms of the ice-covered season length, but the snow accumulation in winter 2014 was minor whereas it was notable in winter 2012 (Table 2). During winter 2014 the maximum SWE was much less (Fig. 6), and the soil frost depth deeper compared to 2011–2013 (Table S1) due to lack of snow and a cold period between 10 January and 8 February 2014, when the mean temperature was -9.0 °C. Thereafter, mean air temperature was warm, i.e. 1.2 °C until the end of March 2014, thus the temperature fluctuated between freeze and thaw. Additionally, the precipitation total in Jan.-May 2014 was larger than in the colder winters of 2011 and 2013, all factors indicated by climate change scenarios for southern Finland.

The cumulative riverine winter/spring loads of TSS, NO<sub>3</sub>-N and organic matter, indicated by COD, only moderately increased during the ice-covered seasons, followed by a sharp increase during the spring thaws 2011–2013 (Fig. 7). As a result of the short frost winters in 2012 and 2014, the riverine loads began to notably increase in March. The cumulative TSS, NO<sub>3</sub>-N and organic matter loads between Nov.-May were the largest by the end of May 2012, since precipitation and  $Q$  were also largest. The cumulative organic matter and TSS yield followed largely the same pattern as the water yield during entire winter/spring (Fig. 7). Instead, the NO<sub>3</sub>-N yield per water yield and flow-weighted mean concentration, were notably high Nov. 2010 – May 2011 compared to other years (Fig. 7).

The ratio of organic matter yield to water yield during the 60 days of freshet was independent of the amount of snow. Instead, the ratio of NO<sub>3</sub>-N load to water yield during freshet 2011–2013 was larger compared to 2014 when the snowpack was thinner. The ratio of TSS load to water yield during freshet 2014 was not significantly different compared to the years 2011–2013 (Fig. 7).

<Figure 6 here please >

<Figure 7 here please>

## 4.2 Event-scale concentration-discharge response variation

The 91 individual storms varied in size ( $Q_{\text{peak}}$ , 2–113  $\text{m}^3 \text{s}^{-1}$ ) and duration (18 h–40 d) (Table 6). In most of the storms at least one parameter showed different hysteretic behaviour compared with the others (Fig. 6). The HI versus  $\Delta C$  unity plane (Fig. 8) illustrates the main differences and similarities in C-Q responses between the variables during the storms. The three parameters are now discussed in more detail.

<Table 6 here please>

<Table 7 here please>

<Figure 8 here please>

### 4.2.1 Turbidity C-Q responses

Anti-clockwise hysteresis in turbidity was the most common in all seasons, except snowmelt periods when clockwise hysteresis dominated. The standard deviation of the turbidity HIs was smaller compared to  $\text{NO}_3\text{-N}$  or COD (Table 6). The anti-clockwise turbidity loops accounted for 54% (49) and clockwise loops 20% (18) of the storms. A synchronised, figure-of-eight or no clear hysteresis occurred in 26% (24) of the storms. The number of cases categorised as no clear hysteresis was 11 (e.g. storms 28, 29, 53, 54, 80 and 85). The mean  $Q_{\text{peak}}$  was smaller during anti-clockwise storms ( $M = 17 \text{ m}^3 \text{s}^{-1}$ ,  $SD = 14 \text{ m}^3 \text{s}^{-1}$ ) compared with clockwise storms ( $M = 55 \text{ m}^3 \text{s}^{-1}$ ,  $SD = 33 \text{ m}^3 \text{s}^{-1}$ ). Flushing ( $\Delta C > 10$ ) of turbid material occurred in most of the storms, i.e. 78% (71) of the cases (Fig 8). Thus, anti-clockwise hysteresis combined with flushing was the dominant C-Q pattern comprising 48% (44) of all storms (Fig. 8). Clockwise hysteresis was found especially when river  $Q$  was large, i.e. usually above  $40 \text{ m}^3 \text{s}^{-1}$  (e.g.

snowmelt storms 9, 30 and 52), or when a low  $Q$  period prevailed before the event (e.g. storms 7, 38, 60 and 61) (Fig. 6). A moderate positive relationship existed between turbidity HIs and  $Q_{\text{peak}}$  of the storms,  $\rho = 0.31$ ,  $p = 0.003$ . The range in storm turbidity correlated overall with the storm  $Q_{\text{peak}}$  ( $\rho = 0.71$ ) in a stronger manner compared with  $\text{NO}_3\text{-N}$  ( $\rho = 0.46$ ) or COD ( $\rho = 0.66$ ), and the relationship was the strongest in the spring (Table 7). A Mann-Whitney test indicated that the average turbidity range was significantly larger in the spring and autumn storms compared with the winter/summer storms,  $U = 483$ ,  $p = 0.000$ , due to the positive relationship between  $Q_{\text{peak}}$  and the turbidity range (Table 7).

The clockwise turbidity peaks preceded the  $Q_{\text{peak}}$ s by on average 12 h ( $SD = 13$  h) in spring and 14 h ( $SD = 6$  h) in autumn. Turbidity peaks described by negative HI values on average lagged the storm  $Q_{\text{peak}}$  by 22 hours ( $SD = 44$  h). The time lag between turbidity and  $Q_{\text{peak}}$  correlated negatively with the  $Q_{\text{peak}}$  values (Table 7) suggesting that larger storm events often resulted in earlier turbidity peaks. HIs for turbidity had a negative relationship with  $Q_{\text{peak}}$  during the summer, since the anti-clockwise hysteresis became stronger as the summer storm  $Q_{\text{peak}}$  increased (Table 7). Conversely, HI for turbidity and storm  $Q_{\text{peak}}$  had a positive relationship during the autumn, since the magnitude of anti-clockwise hysteresis decreased with increasing  $Q$  and clockwise hysteresis was related to large storms. Each spring, the freshet initiated at least one storm with clockwise turbidity hysteresis (Figs. 6 and 10). No clear hysteretic response for turbidity occurred during events with a small discharge range together with a small  $Q_{\text{peak}}$  ( $\leq 10 \text{ m}^3 \text{ s}^{-1}$ ) or when the  $Q_{\text{peak}}$  of an antecedent storm was relatively large.

The number of detected storms during ice-covered period was 10. During those storms turbidity exhibited flushing behaviour ( $\Delta C > 10$ ), but no  $\text{NO}_3\text{-N}$  flushing was detected ( $\Delta C < 10$ ). COD displayed flushing behaviour ( $\Delta C > 10$ ), in only one ice-covered event (storm 51).

Four subsequent spring events (storms 30-33) demonstrated the effect of large antecedent storms on the turbidity C- $Q$  response. A clockwise hysteresis pattern (storms 30 and 31) changed to nearly synchronised behaviour (storm 32) and finally to anti-clockwise in the last storm (33), coupled with a small  $Q_{\text{peak}}$  (Fig. 10).

Turbidity and COD showed more similarities in their behaviour than turbidity and NO<sub>3</sub>-N.

Turbidity and COD were mainly flushing combined with anti-clockwise hysteresis, whereas dilution was common for NO<sub>3</sub>-N (Fig. 8). Turbidity HI's and COD HI's of storms correlated strongly during autumn, winter and spring storms. In addition, the mean turbidity and mean COD concentrations of the storms showed a very strong relationship ( $\rho = 0.93$ ) with each other (Table 7). Overall, the mean turbidity and COD mean concentration values correlated more strongly with the storm  $Q_{\text{peak}}$  compared with NO<sub>3</sub>-N (Table 7), since NO<sub>3</sub>-N mean concentrations had no significant relationship with storm  $Q_{\text{peak}}$ s or  $Q_{\text{range}}$ s in autumn or winter. Turbidity was peaking faster than the COD or NO<sub>3</sub>-N in most of the storms.

<Figure 10 here please>

#### 4.2.2 NO<sub>3</sub>-N C-Q responses

Anti-clockwise hysteretic loops existed for NO<sub>3</sub>-N in 51% (46) and clockwise loops in 23% (21) of the storms (Fig. 8). NO<sub>3</sub>-N and turbidity exhibited coeval anti-clockwise loops in 30 storms. A total of 26% (23) of the HI values of NO<sub>3</sub>-N indicated either a synchronised, figure-of-eight or no clear hysteretic response. Only four of the cases (e.g. storm 28) had no clear hysteretic response. Anti-clockwise NO<sub>3</sub>-N hysteresis was more common during the summer than the winter storms. During the summer, as many as 71% (12 of the total 17) of the storms displayed anti-clockwise NO<sub>3</sub>-N hysteresis, whereas, in winter this was only 24%. Connected to those 12 summer storms ( $Q_{\text{peak}} = 2\text{--}15 \text{ m}^3 \text{ s}^{-1}$ ), most of the turbidity and COD HIs were also anti-clockwise. Flushing ( $\Delta C > 10$ ) of NO<sub>3</sub>-N during the rising limb occurred in 22% (20), and dilution ( $\Delta C < 10$ ) in 17% (15) of the storms. Flushing behaviour was predominantly absent, since in 60% (54) of the storms  $\Delta C$  was negative. Dilution patterns exhibited were related to consecutive storms in the autumn and spring when  $Q_{\text{peak}}$  was large ( $M = 56 \text{ m}^3 \text{ s}^{-1}$ ,  $SD = 19 \text{ m}^3 \text{ s}^{-1}$ ). Within anti-clockwise storms, the average  $Q_{\text{peak}}$  ( $M = 18 \text{ m}^3 \text{ s}^{-1}$ ,  $SD = 16 \text{ m}^3 \text{ s}^{-1}$ ) was smaller than in clockwise events ( $M = 34 \text{ m}^3 \text{ s}^{-1}$ ,  $SD = 34 \text{ m}^3 \text{ s}^{-1}$ ). Accordingly, the NO<sub>3</sub>-N lag correlated negatively with the storm  $Q_{\text{peak}}$

(Table 7). Clockwise hysteresis was mainly related to large spring and autumn Qs but also a few storms with a small  $Q_{\text{peak}}$  had a positive HI e.g. storms 13 and 37 during summer storms 6, 8, 29, 64, 65 and 69 during winter (Fig. 6). No correlation was found between the HI for  $\text{NO}_3\text{-N}$  and storm  $Q_{\text{peak}}$  or  $Q_{\text{range}}$  values. The HI for  $\text{NO}_3\text{-N}$  showed a moderate negative correlation ( $\rho = -0.42$ ) with the range of  $\text{NO}_3\text{-N}$  concentrations during the autumn, thus the  $\text{NO}_3\text{-N}$  concentration change was larger for anti-clockwise storms than for clockwise. The average  $\text{NO}_3\text{-N}$  range was significantly larger in the spring and autumn storms compared to the smaller winter and summer storms,  $U = 616$ ,  $p = 0.005$ . The year 2012 was extremely wet and resulted mainly in dilution patterns for  $\text{NO}_3\text{-N}$  concentrations during the autumn.

The  $\text{NO}_3\text{-N}$  peaks lagged  $Q_{\text{peak}}$  by on average 51 hours ( $SD = 41$  h) in anti-clockwise events. The  $\text{NO}_3\text{-N}$  concentration peaks occurred relatively late after  $Q_{\text{peak}}$  during the growing season, since the average lag times in the anti-clockwise summer and autumn storms were 77 and 42 hours, respectively. Consequently, in the summer there was an additional 1.5-day delay between  $\text{NO}_3\text{-N}$  and  $Q_{\text{peak}}$  compared to the autumn storms. The  $\text{NO}_3\text{-N}$  peaks were often the last to occur compared with turbidity or COD in storm all year round, especially during summer. All three parameters experienced coevally anti-clockwise loops in a total of 26 summer and autumn storms. The median lag time between the concentration and  $Q_{\text{peak}}$ s in those anti-clockwise storms were 15, 27 and 43 hours for turbidity, COD and  $\text{NO}_3\text{-N}$  respectively. In a few autumn storms COD flushed and  $\text{NO}_3\text{-N}$  diluted; thus the largest  $\text{NO}_3\text{-N}$  concentration occurred before the COD peak.

#### 4.2.3 COD C-Q responses

Anti-clockwise behaviour was the most common for COD, comprising 77% (68) of the storms. Clockwise hysteresis accounted for 15% (13) of the storms, and 7% (6) of the cases had synchronised or figure-of-eight C-Q response, which occurred through all seasons (Fig. 8). It was only during one storm (storm 76) that COD had no clear hysteresis. The mean  $Q_{\text{peak}}$  in anti-clockwise storms ( $M = 26 \text{ m}^3 \text{ s}^{-1}$ ,  $SD = 25 \text{ m}^3 \text{ s}^{-1}$ ) was larger than in clockwise storms ( $M = 17 \text{ m}^3 \text{ s}^{-1}$ ,  $SD = 26 \text{ m}^3 \text{ s}^{-1}$ ). There were no detectable seasonal differences in the HIs of COD, since during every season >70% of the HIs were

negative (Fig. 8). Flushing ( $\Delta C > 10$ ) behaviour occurred in 45% (40) of the storms. There were no storms that diluted COD ( $\Delta C < -10$ ). During the large snowmelt storms in 2011–2013, the COD peaks were the last to occur (Fig. 9). Overall, COD had the most uniform C-Q response pattern compared with  $\text{NO}_3\text{-N}$  and turbidity, since in 77% of the storms the hysteretic response was anti-clockwise along with flushing behaviour (Fig. 8). Thus, the mean HI for COD ( $M = -0.29$ ,  $SD = 0.35$ ) was significantly smaller compared to the mean HI for turbidity ( $M = -0.13$ ,  $SD = 0.27$ ),  $U = 2615$ ,  $p = 0.000$ , or  $\text{NO}_3\text{-N}$  ( $M = -0.16$ ,  $SD = 0.32$ ),  $U = 2913$ ,  $p = 0.002$ .

<Figure 9, here please>

The average COD storm peak and range values were largest during autumn storms (Table 6). The average range of COD in autumn storms was significantly larger compared to spring storms,  $U = 187$ ,  $p = 0.042$ , whereas  $Q_{\text{peak}}$  was not significantly different between autumn and spring storms. Anti-clockwise COD peaks lagged storm  $Q_{\text{peak}}$  by, on average 42 hours ( $SD = 26$  h) in the spring, 18 hours ( $SD = 24$  h) in the autumn, and 41 hours ( $SD = 56$  h) in the summer. HI for COD had a negative relationship with  $Q_{\text{peak}}$  during the summer (Table 6). Four clockwise storms occurred at low  $Q_s$  ( $< 5 \text{ m}^3 \text{ s}^{-1}$ ), and anti-clockwise hysteresis tended to get stronger as storm  $Q_{\text{peak}}$  increased in summer.

## 5. Discussion

### 5.1 Interannual and seasonal water quality variation

The annual and freshet period TSS,  $\text{NO}_3\text{-N}$  and organic carbon loads were the highest during the wettest year consistent with earlier studies (e.g. Davis et al., 2014). Large TSS  $\text{NO}_3\text{-N}$  and COD concentrations during autumn and spring thaw periods indicated river bed erosion, surface flushing, soil leaching of

NO<sub>3</sub>-N and low NO<sub>3</sub>-N uptake via biological activity. The risk of NO<sub>3</sub>-N leaching from the catchment to the river increases during wet conditions when the vegetation is not efficiently using the available mineral N (Øygarden et al., 2014). The NO<sub>3</sub>-N concentrations were at their lowest during summer. This was consistent with Laznik et al. (1999), and indicated effective microbiological immobilisation of the mineral N, intensified denitrification and N uptake by plants. The high TSS concentrations during summer 2014 may have been influenced by small quantities of spring freshet flushing in 2014.

The average COD storm concentrations and ranges were the largest during autumn. This was likely due to a combination of increased hydraulic connectivity and large pools of organic matter available from the soil surface and shallow soils produced through microbiological decomposition and leaf fall. Supporting our COD results, the largest carbon (DOC, TOC) concentrations in rivers have been previously reported during the autumn (Lepistö et al., 2008; Mattsson et al., 2015; Strohmeier et al., 2013). Hence, the autumn storms seem to flush organic matter most effectively, which is contradictory to result by Blaen et al. (2017) who reported declining DOC levels through autumn from an agricultural site. Some earlier studies report larger DOC concentrations for spring than autumn, since the freshet Q magnitude is larger than that of autumn (e.g. Guo et al., 2012; Qiao et al., 2017). It has been suggested that agricultural residues breakdown under the snowpack and intensify DOC flushing during snowmelt (Qiao et al., 2017). Our results suggest that the ratio of organic matter freshet yield to water yield is similar interannually and therefore not dependent on snowpack existence. DOC concentrations are typically the highest in surface soil layers, and thus the surface runoff and seepage from organic soils contribute to riverine DOC concentrations. In general, DOM concentrations are larger in forest than arable soils due to the different vegetation types (Chantigny, 2003). In our studied catchment, large areas are forest and probably contribute substantially to the seasonal COD variations. During the frozen season, COD concentrations mainly decreased, similar to earlier DOC studies (Sebestyen et al., 2008; Guo et al., 2012), indicating that the influence of point sources was not significant. The monthly average COD concentrations were the lowest in the summer each year. Possible explanations are that organic matter removal by plants (Taylor et al., 2011) was enhanced during summer or organic matter storages were



depleted through winter and spring flushing events. The results by Guo et al. (2012) contrast with our findings as they reported that organic carbon had the lowest concentrations during the ice-covered season in the much larger Yukon River. These results highlight the differences between the seasonal dynamics of organic matter concentrations, coupled with differences in hydrographs, in two rivers which experience ice-covered periods.

The river when ice-covered was less turbid in contrast to open-water river with equivalent discharges ( $Q < 10 \text{ m}^3/\text{s}$ ). The phenomenon is most likely explained by in-stream processes, namely reduced shear stress towards the river bed due to ice cover, since particle flushing rates from the catchment was expected to be small both in ice-covered and vegetated seasons, as  $Q_s$  were not high. River ice reducing bed shear stress has been previously detected in flume studies (Lau and Krishnappan, 1985; Muste et al., 2000) and from field grab sampling followed by numerical modelling (Kämäri et al., 2015; Shakibaeinia et al., 2017). Ice cover reduces the bedload transport rates according to Smith and Ettema (1995) and our result suggests that ice cover also reduces the rivers transport capacity of TSS.

Decreases in  $\text{NO}_3\text{-N}$  concentrations during the ice-covered periods indicated that groundwater sources diluted the in-stream concentrations. There was no consistent indication of flushing of COD or  $\text{NO}_3\text{-N}$  ( $\Delta C > 10$ ) from the catchment soils or through runoff during the ice-covered river storms. Under warmer climate conditions and shortened ice-covered periods, the event scale flushing may become more frequent in current ice-covered months. Thus, this results in changes to seasonal water quality and shifts in the timing of riverine loads.

## 5.2 Event-scale concentration-discharge response

Anti-clockwise hysteresis was dominant for turbidity,  $\text{NO}_3\text{-N}$  and COD. This is likely to be because the  $Q$  wave triggered by the storm tends to travels faster than the mean channel flow velocity and for example suspended sediments tend to travel at a speed that is closer to the mean flow velocity, hence resulting the lag between  $Q$  and turbidity peaks (Bull, 1997; Williams, 1989). The  $Q$  wave is the wavefront, shown by



an increase in stage at a particular site. The turbidity,  $\text{NO}_3\text{-N}$  and COD lags were inversely related to storm magnitude, which has been previously reported for the natural chemical concentrations of river water (Walling and Foster, 1975). The observed, generally slower peaking  $\text{NO}_3\text{-N}$  compared to COD or turbidity could be explained by  $\text{NO}_3\text{-N}$  and organic matter arriving in the river from different sources and also that the availability of  $\text{NO}_3\text{-N}$  and organic matter to mobilise varies on an event basis as well as seasonally. Several issues in the detected storm C-Q response of the solutes suggest similarities in export dynamics for turbidity and dissolved organic matter, whereas the C-Q response of  $\text{NO}_3\text{-N}$  was often different compared to turbidity or COD. Storm C-Q response findings by Cerro et al. (2014) contrast to ours, since they found the most similarities between the behaviour of soluble  $\text{NO}_3\text{-N}$  and DOC and between particulate organic carbon and suspended solids. In the Vantaa River  $\text{NO}_3\text{-N}$  and COD behaved similarly and experienced both anti-clockwise hysteresis and flushing only in 24% (21 storms) of the events but turbidity and COD in as many as 44% (38 storms) of the storms. However, the determined COD data may contain some amount of particulate organic matter, since there is a relationship between COD and TOC (Kortelainen, 1993). The 'raw' TOC was also measured in the site 1 (unpublished data) and it showed sharper peaks compared to 'raw' DOC.

The few identified turbidity and  $\text{NO}_3\text{-N}$  clockwise loops were common during large spring and autumn storms, whereas a similar effect was not detected for COD. The strength of the clockwise hysteresis was on average weaker for all parameters compared with the wider anti-clockwise loops. The sediment wave may move faster than the Q wave in an event where sediment is readily available for transport. Therefore, clockwise hysteresis may appear if the peak TSS concentration is produced by the wavefront transporting sediment rather than the maximum  $Q_{\text{peak}}$  (Bull, 1997), which likely occurred at the site studied, e.g. during the intensive spring snowmelt storms. The clockwise turbidity and  $\text{NO}_3\text{-N}$  hysteresis indicates a finite source of material for flushing, related to the size of the discharge peak (Williams, 1989) as well as rapid in-channel, bank-derived or nearby field drains-derived mobilisation (Bowes et al., 2005; Seeger et al., 2004). Consequently, the HI for turbidity correlated positively with the storm  $Q_{\text{peak}}$  during autumn, consistent with Bieroza and Heathwaite (2015). The analysis indicates

increased drag forces during rising limbs and rapid mobilisation of bed sediments, since turbidity peaked most often prior to  $\text{NO}_3\text{-N}$  or COD. There was no evidence that significant amounts of  $\text{NO}_3\text{-N}$  or organic matter were mobilised from the river bed associated with discharge increase, since during ice-covered periods, flushing of  $\text{NO}_3\text{-N}$  or organic matter indicated by COD was minimal, whereas the flushing of turbid material did occur. Lloyd et al. (2016c) reported for a small headwater catchment that clockwise turbidity hysteresis was associated with either the largest storms or smaller events which occurred after periods of low Q. The larger Vantaa River behaved similarly. Contradictory to the site studied, clockwise hysteresis has been predominantly reported for TSS, and it has been suggested to occur as sediments flush from the channel or near stream zones (Cerro et al., 2014; Seeger et al., 2004) or due to bank erosion (Bull, 1997; Smith and Dragovich, 2009). Within the site studied, the storms which showed no clear turbidity hysteresis, overall had a  $Q_{\text{range}}$  less than  $4 \text{ m}^3 \text{ s}^{-1}$ , and  $Q_{\text{peak}}$  of antecedent storms were at least three times larger. Consequently, the unclear hysteresis events could be explained by the fact that there was a lack of fine bed sediments to be mobilised. Overall the C-Q pattern of turbidity varied between storm events, which has been reported earlier for suspended solids and for phosphorus (P) (e.g. Bierozza and Heathwaite, 2015; Bowes et al., 2005; Lloyd et al., 2016c; Valkama et al., 2017). We found factors such as the storm size, ice-cover existence and the size and timing of antecedent storms impacted C-Q patterns.

A decrease in catchment size and increase in the area used for agriculture supports the occurrence of more rapid turbidity peak and clockwise hysteresis based results presented herein and the study by Valkama and Ruth (2017). In a small agriculturally intensive headwater site in the same Vantaa River catchment, clockwise TP hysteresis was predominant (Valkama and Ruth, 2017) whereas at a larger mixed land-use site – i.e. the downstream site 1 of the Vantaa River – the turbidity hysteresis was predominantly anti-clockwise. Thus, supporting the suggestion that increasing the intensity of agricultural activity promotes and increases the magnitude of clockwise hysteresis (Bowes et al., 2005; Lloyd et al., 2016c) for the Vantaa River catchment. In addition, the above-mentioned slower velocity of suspended solids with respect to wave velocity causes the solute peak lag time to increase with distance downstream

(Heidel, 1956; Williams, 1989). Lloyd et al. (2016c) reported predominantly clockwise turbidity hysteresis form a surface water-dominated headwater catchment and anti-clockwise hysteresis for a larger groundwater dominated chalk catchment. For this reason, the catchment size, distance from solute source areas, catchment hydrology and land use all play a role in observed turbidity lag and in the direction of hysteresis.

Similar to our COD results, Strohmeier et al. (2013) reported exclusively anti-clockwise loops for DOC from a small forested catchment. Storm COD HI versus COD flushing index pattern (Fig. 8) was similar to DOC behaviour reported by Vaughan et al. (2017) from three sites under varying land use. Whereas Blaen et al., (2017) reported more clockwise than anti-clockwise DOC hysteresis from a headwater agricultural catchment. The share of organic soil is a stronger predictor of DOC concentration than land use (Autio et al., 2016) and is likely one factor influencing on reported variable DOC and COD HIs from different sites. The influence of point sources of P and organic matter (indicated by turbidity and COD) can be interpreted to be small in the Vantaa River, since turbidity and COD levels predominantly increased at the rising limb. Instead, clockwise P hysteresis combined with strong dilution patterns during increases in Q indicate non-rain-related inputs from sewage treatment plants in a study by Bowes et al. (2015). Turbidity and COD levels had a positive relationship with storm size, consistent with earlier and commonly reported connections between Q increases and flushing of DOC or turbid material (e.g. Bieroza and Heathwaite, 2015; Blaen et al., 2017; Butturini et al., 2006; Cerro et al., 2014; Moatar et. al., 2017; Vaughan et al., 2017).

The dilution pattern of  $\text{NO}_3\text{-N}$  during consecutive storms was an indication of exhaustion of  $\text{NO}_3\text{-N}$  from diffuse rather than point sources, since the  $\text{NO}_3\text{-N}$  concentrations did not increase during baseflow. Previous studies have found evidence of exhaustion of  $\text{NO}_3\text{-N}$  sources following consecutive storms or wet periods (Bende-Michl et al., 2013; Blaen et al., 2017; Outram et al., 2014). This suggests that  $\text{NO}_3\text{-N}$  rich pore water is flushed from the soil at a fast rate and organic N mineralisation and nitrification rates are not able to maintain the  $\text{NO}_3\text{-N}$  concentrations. Autumn is typically a wet period and the dilution of  $\text{NO}_3\text{-N}$  took place in some of the storms. Accordingly, results of Davis et al. (2014) from

an agricultural watershed suggest that wet antecedent conditions promote dilution of  $\text{NO}_3\text{-N}$  during individual rainfall events. Predominantly anti-clockwise  $\text{NO}_3\text{-N}$  hysteresis has been reported from a small Portuguese mixed land-use catchment (Ramos et al., 2015), but almost exclusively clockwise  $\text{NO}_3\text{-N}$  hysteresis and dilution of  $\text{NO}_3\text{-N}$  was observed in all seasons in catchments where rainfall diluted nitrate (Bowes et al., 2015; Lloyd et al., 2016c).

In general, season, rainfall, subsurface hydrologic connectivity and agricultural cropping systems as well as the rate and timing of the fertiliser application highly influence N losses and  $\text{NO}_3\text{-N}$  C-Q relationship in tile drained fields (Randall and Mulla, 2001; Stenberg et al., 2012). Within the basin studied here, the nutrient application on fields is usually carried out after the snowmelt in May when soils have dried enough and allows sowing. Rainfall soon after fertiliser application causes  $\text{NO}_3\text{-N}$  leaching from fields and rapid nutrient concentration peaks in the headwaters of the basin (unpublished data from the Lepsämäenjoki River at the Vantaa River headwaters). However, clockwise  $\text{NO}_3\text{-N}$  hysteresis was not observed during such storms in May or June at this downstream site.

### 5.3 Response of turbidity, $\text{NO}_3\text{-N}$ and COD to snowmelt

Turbidity,  $\text{NO}_3\text{-N}$  and COD were flushed during the rising limb of the large snowmelt storms (storms 9, 30 and 52) (see Figs. 9 and 10) during the years 2011–13 which had marked snow accumulation. Flushing indicated that in the initial snowmelt phase, plenty of sediment,  $\text{NO}_3\text{-N}$  and organic matter was mobilised from near stream areas via surficial quick flow pathways, along with the remobilisation of bed sediments. Additionally, melt water contained deposited atmospheric N, which likely had some influence on riverine  $\text{NO}_3\text{-N}$  concentrations (Pellerin et al., 2012; Sebestyen et al., 2008). All freshet storms shown in Fig. 10 were flushing ( $\Delta C > 0$ ) suspended solids and COD related material. Four consecutive events (storms 30–33), flushing of  $\text{NO}_3\text{-N}$  occurred only during the first event (storm 30) and thereafter  $\text{NO}_3\text{-N}$  was diluting (storms 31, 32). Consistent with our results, flushing behaviour for DOC has been reported from other forested and agricultural sites (e.g. Ågren et al., 2008; Vaughan et al., 2017). Clockwise turbidity

679 hysteresis showed during snowmelt (storms 9, 30, 31 and 52) has been previously reported (Gonzales-  
680 Inca et al., 2018; Tananaev and Debolskiy, 2014) and may indicate rapid bed sediment remobilisation or  
681 bank erosion.

682 Results suggest that ice clearance and in-stream physical processes affected the turbidity C-  
683 Q response. The snowmelt hydrographs generally exhibited two distinct turbidity peaks prior to one  
684 snowmelt  $Q_{\text{peak}}$  in 2011 and 2013 (storms 9, 52), which might be because break-up of river ice introduced  
685 increased scour which increased turbidity and resulted in an additional turbidity peak (Beltaos 2016;  
686 Scrimgeour et al., 1994). During storms 9 and 52, the first turbidity peak occurred five and six days prior  
687 to  $Q_{\text{peak}}$ , respectively.

688 We observed clockwise or synchronised  $\text{NO}_3\text{-N}$  and turbidity hysteresis along with flushing  
689 behaviour during the early phase of snowmelt, but the COD hysteresis was anti-clockwise in each of the  
690 three largest snowmelt storms 9, 30 and 52 (Fig. 10). The C-Q response suggests flushing of a finite  
691 source of  $\text{NO}_3\text{-N}$  from soil and snowpack into the river (Ohte et al., 2004; Pellerin et al., 2012; Zhao et  
692 al., 2017) and that unfrozen soil  $\text{NO}_3\text{-N}$  pools have gradually increased under the snowpack. The result  
693 does not support the suggestion by Brooks et al. (1998) that microbial biomass developed in snow-  
694 covered soil acted as a significant buffer limiting  $\text{NO}_3\text{-N}$  flushing from soils into surface waters during  
695 early snowmelt.

696 The amount of atmospheric  $\text{NO}_3\text{-N}$  deposition can contribute substantially to the elevated  
697  $\text{NO}_3\text{-N}$  concentrations observed in the river water during the early phase of snowmelt especially in  
698 forested sites with low baseflow  $\text{NO}_3\text{-N}$  concentrations (Casson et al., 2014; Pellerin et al., 2012). The  
699 relationship between atmospheric N and soil-nitrified  $\text{NO}_3\text{-N}$  mobilised by percolating meltwater has  
700 been intensively studied in the forested Sleepers River watershed in Vermont U.S. Ohte et al. (2004) have  
701 observed that atmospheric  $\text{NO}_3\text{-N}$  can be temporarily the dominant contributor to the elevated  
702 concentrations but soil-derived  $\text{NO}_3\text{-N}$  produced via nitrification was the dominant source through the  
703 entire snowmelt season studied in Sleepers River (Pellerin et al., 2012). In addition, Sebestyen et al.  
704 (2008) reported that after the onset of snowmelt, the majority of  $\text{NO}_3\text{-N}$  in surficial soil waters originated

from atmospheric sources, with a fraction of atmospheric N directly delivered to the stream. The atmospheric inorganic N deposition observed in the southern Finland is about  $3 \text{ kg N ha}^{-1} \text{ y}^{-1}$  (2003–2011) (Ruoho-Airola et al., 2014) and  $4\text{--}5 \text{ kg N ha}^{-1} \text{ y}^{-1}$  (2000–2014) in the northeastern USA (NADP, 2017). The winter baseflow  $\text{NO}_3\text{-N}$  concentration was higher and the atmospheric N deposition was lower in the Vantaa River than in Sleepers River. The  $\text{NO}_3\text{-N}$  concentration increased sharply  $1.8\text{--}3.9 \text{ mg L}^{-1}$  during the initial snowmelt phase of the three large snowmelt storms in the Vantaa River. However, the storms during the later stage of snowmelt during 2012 were not able to increase the  $\text{NO}_3\text{-N}$  concentration compared with the initial snowmelt pulse. In addition, during the autumn storms it was typical that the  $\text{NO}_3\text{-N}$  peak occurred last, but in contrast, during the snowmelt storms the  $\text{NO}_3\text{-N}$  peaked earlier than COD, indicating that  $\text{NO}_3\text{-N}$  deposited in the snow caused the initial  $\text{NO}_3\text{-N}$  peak to arrive prior to COD. Thus, the observed clockwise or synchronized  $\text{NO}_3\text{-N}$  hysteresis pattern and flushing (storms 9, 30 and 52) suggests a contribution of atmospherically deposited  $\text{NO}_3\text{-N}$  during the initial snowmelt phase and/or finite sources of  $\text{NO}_3\text{-N}$  in surficial soils during the entire snowmelt, which was reflected as a dilution pattern of  $\text{NO}_3\text{-N}$  during the later sequential snowmelt storm events (storms 31, 32) (Figs. 9 and 10). During storm 33, the snow had already entirely melted and the slight  $\text{NO}_3\text{-N}$  flushing may be related to enhanced soil N mineralisation rate as spring progressed. We assume that the pulse of direct atmospheric  $\text{NO}_3\text{-N}$  played a role in this catchment during the initial snowmelt phase and during the entire snowmelt period the amount of  $\text{NO}_3\text{-N}$  nitrified in the soil under snowpack was mainly influencing the C-Q pattern of  $\text{NO}_3\text{-N}$  (Kendall et al., 1995). In the studied basin, the main contributor to the annual riverine  $\text{NO}_3\text{-N}$  loads is soil-derived  $\text{NO}_3\text{-N}$  from agricultural areas (Vuorenmaa et al., 2002).

During sequential snowmelt storms, the COD dynamics were more tightly coupled with the streamflow than that of  $\text{NO}_3\text{-N}$ , which is consistent with other published studies (Pellerin et al., 2012; Sebestyen et al., 2008). However, the COD concentrations did not return to initial levels preceding the large snowmelt storms. In general, during the falling limb of the snowmelt flow peaks, turbidity and  $\text{NO}_3\text{-N}$  levels decreased faster than that of COD (Fig. 9). Thus, in the latter stage of snowmelt the water percolating through surficial soil was presumably rich in organic matter and maintained the COD

concentrations longer than turbidity or  $\text{NO}_3\text{-N}$ . We expect the snowmelt water mainly flushed organic matter from near-surface and shallow subsurface flowpaths into the river. Boyer et al. (1997) showed similarly that flushing of the material and the resultant increase in COD from riparian soils began on the rising limb and continued beyond the recession of the first snowmelt flow peak. However, COD flow-weighted mean concentrations were larger in autumn than spring. The results of Lepistö et al. (2008) were similar, but it remained unclear as to whether the snowmelt water partly diluted DOC levels and prevented DOC concentrations reaching as high as during autumn, or if the soil pool of organic matter available for transportation was smaller during spring than autumn.

#### **5.4 Implications of warmer winters on concentrations and loads**

Interannually contrasting winter temperature and snow conditions presented an opportunity to examine snowpack and soil frost conditions on solute concentrations. Spring 2014 was lacking a large snowmelt event and the smaller freshet storms (71–77) mainly diluted  $\text{NO}_3\text{-N}$  concentration. The  $\text{NO}_3\text{-N}$  concentration experienced only a moderate increase after the ice clearance in March 2014 and did not rise as high as during the spring thaw in 2010–2013, which might have been influenced by the deeper than the average soil frost depth during February 2014 (Table S1) (Zhao et al., 2017). The results are inconsistent compared to those reported by Fitzhugh et al. (2001) who found that soil freezing accelerated  $\text{NO}_3\text{-N}$  leaching from forests.

The lack of snow in 2014 had the most influence on the freshet period dynamics of  $\text{NO}_3\text{-N}$ , since the typical snowmelt related flushing pattern for  $\text{NO}_3\text{-N}$  was not observed there (Figs. 9 and 10). TSS and COD loads over winter and spring were more tightly coupled with Q, but  $\text{NO}_3\text{-N}$  loads seem to be notably affected by other contributing factors like soil hydrology and N mineralisation processes. However, the largest summer monthly flow-weighted TSS concentrations in 2014 may have been partly due to the lack of a large snowmelt Q event and related reduction in bed material flushing. The data does not support the idea that precipitation falling more as rain than snow



during winter would increase TSS, NO<sub>3</sub>-N or COD losses from the rivers to the seas. Presumably because snowmelt storms initiate large material fluxes. Surface runoff is the major flow pathway for sediment export based on the catchment modelling by Adams et al. (2016) and was likely increased during intensive snowmelt storms in the Vantaa River basin. Haei et al. (2010) conducted field scale experiments in a forested site and suggested that deeper and longer soil frost results in higher DOC losses from catchments to streams during snowmelt. Their results are not supported by this study, since organic matter yield, indicated by COD, per water yield was equal between the years when an extensive snowpack was insulating and preventing the development of soil frost and during the year with remarkable soil frost.

Water quality and riverine loads are influenced by changes in evapotranspiration, and the amount of surface flushing and seepage through soil, as well as biogeochemical processes like the relationship between soil freezing and river chemistry (Fitzhugh et al., 2003). In future climate conditions, moderate increases in annual average Q, inorganic N and TSS loads are projected for the Vantaa River sub-basin (Rankinen et al., 2013). Storm-dependent nutrient transport has been reported, e.g. by Outram et al. (2014) from rural catchments and consistently we found that the storm loads correlated strongly and positively with storm  $Q_{\text{peakS}}$  (Table 7). It has been speculated that the warmer winters driven by climate change, along with higher rainfall volumes and intensities could cause intensified nutrient leaching from arable land (Ockenden et al., 2016; Puustinen et al., 2007). More long-term research should be carried out in watersheds that are experiencing interannually variable SWE and winter temperatures. Such studies would reveal the impacts that the shift from snow dominated winter conditions to a freeze-thaw regime has in terms of water quality and finally on the seasonal and annual material loads in cold climate mixed land-use catchments that drain into the seas.

## 6. Conclusions

The present study is the first to present the C-Q response of turbidity, NO<sub>3</sub>-N and COD over four years of hourly monitoring in a mixed land-use, cold climate watershed affected by seasonal snow accumulation



and river ice cover. The distinct C-Q response of the solutes suggested differences in sources and the availability of transportable material. The ice-cover reduced turbidity during the winter baseflow compared to with open channel conditions. However, a similar effect was not detected for  $\text{NO}_3\text{-N}$  or COD. The flushing of COD related organic matter was the largest during autumn storms. Conversely, TSS concentrations and its flushing behaviour were similar during autumn and spring. Overall, COD and turbidity had similar C-Q behaviours featuring predominantly anti-clockwise hysteresis and flushing patterns, but the C-Q response of  $\text{NO}_3\text{-N}$  was markedly more variable, since dilution was also common during the storms.  $\text{NO}_3\text{-N}$  flushing from the catchment substantially varies seasonally, being the largest in the early phase of snowmelt and dormant periods. However, dilution of  $\text{NO}_3\text{-N}$  in river water was observed during large storm events in the autumn and during spring storms when the preceding winter experienced very little snow accumulation. The results suggest that a thick snowpack and related unfrozen ground beneath the snow increases  $\text{NO}_3\text{-N}$  availability for spring-time flushing. Turbidity overall peaked most rapidly and  $\text{NO}_3\text{-N}$  the slowest during storm events.

Our findings suggest substantial changes in seasonal distribution of material losses and water quality due to climate change. Reduced ice-covered period impacts on river channel sediment dynamics. Increased turbidity and TSS transportation at winter low flows are expected as bed shear stress increases in open water river compared to ice-covered. However the impact of that effect on annual sediment yields is minor as the yield is low at winter baseflows. Contradictorily, more precipitation falling as rain instead of snow distributes the typical large snowmelt related sediment, organic matter, and  $\text{NO}_3\text{-N}$  losses over the entire winter and spring period in case the large snowmelt storms vanish. We found no evidence that a warmer winter with less snow would increase suspended sediment, organic matter or  $\text{NO}_3\text{-N}$  load per water yield at seasonal winter-spring period or at annual scales. Lack of intensive snowmelt induced sediment flush may have implications on water quality beyond the melt season and increase suspended sediment concentrations during the summer which was observed in the studied site.

## Acknowledgements

This work was supported by the Academy of Finland [ExRIVER, grant number 267345]; the Maj and Tor Nessling Foundation [grant numbers 201300067, 201500046, 201600042]; Finnish Cultural Foundation, Satakunta Regional Fund [grant number 75162329] and the Emil Aaltonen Foundation. The Pitkälampi in-situ monitoring was initiated under the Baltic Sea Region Programme's project: 'Comprehensive Policy Actions and Investments in Sustainable Solution in Agriculture in the Baltic Sea Region'. The authors wish to thank the EU Baltic Sea Region Programme 2007–2013 [Baltic COMPASS, project number 040] and the Tekes project CLEEN/MMEA for the funding the monitoring. The constructive criticism and valuable advices from three anonymous reviewers and the Journal of Hydrology Editorial team are greatly acknowledged.

## 11. References

- Adams, R. et al., 2016. Simulating high frequency water quality monitoring data using a catchment runoff attenuation flux tool (CRAFT). *Sci. Total Environ.*, 572: 1622-1635. DOI:<http://doi.org/10.1016/j.scitotenv.2016.01.045>
- Gonzales-Inca, C. et al., 2018. Spatial modeling of sediment transfer and identification of sediment sources during snowmelt in an agricultural watershed in boreal climate. *Sci. Total Environ.*, 612: 303-312. DOI:<https://doi.org/10.1016/j.scitotenv.2017.08.142>
- Ågren, A. et al., 2008. Dissolved organic carbon characteristics in boreal streams in a forest-wetland gradient during the transition between winter and summer. *Journal of Geophysical Research: Biogeosciences*, 113(G03031).
- Autio, I., Soinne, H., Helin, J., Asmala, E., Hoikkala, L., 2016. Effect of catchment land use and soil type on the concentration, quality, and bacterial degradation of riverine dissolved organic matter. *Ambio*, 45(3): 331-349. DOI:[10.1007/s13280-015-0724-y](https://doi.org/10.1007/s13280-015-0724-y)

- 834 Beltaos, S., 2016. Extreme sediment pulses during ice breakup, Saint John River, Canada. *Cold Reg. Sci.*  
 835 *Technol.*, 128: 38-46. DOI:<http://dx.doi.org/10.1016/j.coldregions.2016.05.005>
- 836 Bende-Michl, U., Verburg, K., Cresswell, H.P., 2013. High-frequency nutrient monitoring to infer  
 837 seasonal patterns in catchment source availability, mobilisation and delivery. *Environ. Monit.*  
 838 *Assess.*, 185(11): 9191-9219. DOI:10.1007/s10661-013-3246-8
- 839 Bieroza, M.Z., Heathwaite, A.L., 2015. Seasonal variation in phosphorus concentration–discharge  
 840 hysteresis inferred from high-frequency in situ monitoring. *J. Hydrol.*, 524: 333-347.  
 841 DOI:<http://dx.doi.org/10.1016/j.jhydrol.2015.02.036>
- 842 Blaen, P.J. et al., 2016. Real-time monitoring of nutrients and dissolved organic matter in rivers:  
 843 Capturing event dynamics, technological opportunities and future directions. *Sci. Total Environ.*,  
 844 569–570: 647-660. DOI:<http://dx.doi.org/10.1016/j.scitotenv.2016.06.116>
- 845 Blaen, P.J. et al., 2017. High-frequency monitoring of catchment nutrient exports reveals highly variable  
 846 storm event responses and dynamic source zone activation. *J. Geophys. Res.: Biogeosci.*, 122(9):  
 847 2265-2281.
- 848 Bowes, M.J., House, W.A., Hodgkinson, R.A., Leach, D.V., 2005. Phosphorus–discharge hysteresis  
 849 during storm events along a river catchment: the River Swale, UK. *Water Res.*, 39(5): 751-762.  
 850 DOI:<http://dx.doi.org/10.1016/j.watres.2004.11.027>
- 851 Bowes, M.J. et al., 2015. Characterising phosphorus and nitrate inputs to a rural river using high-  
 852 frequency concentration–flow relationships. *Sci. Total Environ.*, 511: 608-620.  
 853 DOI:<http://dx.doi.org/10.1016/j.scitotenv.2014.12.086>
- 854 Boyer, E.W., Hornberger, G.M., Bencala, K.E., McKnight, D.M., 1997. Response characteristics of DOC  
 855 flushing in an alpine catchment. *Hydrol. Process.*, 11(12): 1635-1647. DOI:10.1002/(SICI)1099-  
 856 1085(19971015)11:12<1635::AID-HYP494>3.0.CO;2-H
- 857 Brooks, P.D. et al., 2011. Carbon and nitrogen cycling in snow-covered environments. *Geogr. Compass*,  
 858 5(9): 682-699.

- 859 Brooks, P.D., Williams, M.W., 1999. Snowpack controls on nitrogen cycling and export in seasonally  
860 snow-covered catchments. *Hydrol. Process.*, 13(14): 2177-2190.
- 861 Brooks, P.D., Williams, M.W., Schmidt, S.K., 1998. Inorganic nitrogen and microbial biomass dynamics  
862 before and during spring snowmelt. *Biogeochemistry*, 43(1): 1-15.  
863 DOI:10.1023/a:1005947511910
- 864 Brown, R.D., Mote, P.W., 2009. The response of Northern Hemisphere snow cover to a changing climate.  
865 *J. Clim.*, 22(8): 2124-2145.
- 866 Brown, R.D., Robinson, D.A., 2011. Northern Hemisphere spring snow cover variability and change over  
867 1922–2010 including an assessment of uncertainty. *The Cryosphere*, 5(1): 219-229.  
868 DOI:10.5194/tc-5-219-2011
- 869 Bull, L.J., 1997. Relative velocities of discharge and sediment waves for the River Severn, UK. *Hydrol.*  
870 *Sci. J.*, 42(5): 649-660. DOI:10.1080/02626669709492064
- 871 Butturini, A., Alvarez, M., Bernal, S., Vazquez, E., Sabater, F., 2008. Diversity and temporal sequences  
872 of forms of DOC and NO<sub>3</sub>-discharge responses in an intermittent stream: Predictable or random  
873 succession? *J. Geophys. Res.: Biogeosci.*, 113, G03016. DOI:10.1029/2008JG000721
- 874 Butturini, A., Gallart, F., Latron, J., Vazquez, E., Sabater, F., 2006. Cross-Site Comparison of Variability  
875 of DOC and Nitrate c-q Hysteresis during the Autumn-Winter Period in Three Mediterranean  
876 Headwater Streams: A Synthetic Approach. *Biogeochemistry*, 77(3): 327-349.
- 877 Campbell, J.L., Reinmann, A.B., Templer, P.H., 2014. Soil freezing effects on sources of nitrogen and  
878 carbon leached during snowmelt. *Soil Sci. Soc. Am. J.*, 78(1): 297-308.
- 879 Cassidy, R., Jordan, P., 2011. Limitations of instantaneous water quality sampling in surface-water  
880 catchments: Comparison with near-continuous phosphorus time-series data. *J. Hydrol.*, 405(1–2):  
881 182-193. DOI:http://dx.doi.org/10.1016/j.jhydrol.2011.05.020
- 882 Casson, N., Eimers, M., Watmough, S., 2014. Sources of nitrate export during rain-on-snow events at  
883 forested catchments. *Biogeochemistry*, 120(1-3): 23-36.

- 884 Cerro, I., Sanchez-Perez, J.M., Ruiz-Romera, E., Antigüedad, I., 2014. Variability of particulate (SS,  
885 POC) and dissolved (DOC, NO<sub>3</sub>) matter during storm events in the Alegria agricultural  
886 watershed. *Hydrol. Process.*, 28(5): 2855-2867. DOI:doi:10.1002/hyp.9850
- 887 Chantigny, M.H., 2003. Dissolved and water-extractable organic matter in soils: a review on the influence  
888 of land use and management practices. *Geoderma*, 113(3–4): 357-380.  
889 DOI:http://dx.doi.org/10.1016/S0016-7061(02)00370-1
- 890 Davis, C.A. et al., 2014. Antecedent Moisture Controls on Stream Nitrate Flux in an Agricultural  
891 Watershed. *J. Environ. Qual.*, 43: 1494-1503. DOI:10.2134/jeq2013.11.0438
- 892 Finlay, J., Neff, J., Zimov, S., Davydova, A., Davydov, S., 2006. Snowmelt dominance of dissolved  
893 organic carbon in high-latitude watersheds: Implications for characterization and flux of river  
894 DOC. *Geophys. Res. Lett.*, 33, L10401. DOI:10.1029/2006GL025754
- 895 Fitzhugh, R.D. et al., 2001. Effects of soil freezing disturbance on soil solution nitrogen, phosphorus, and  
896 carbon chemistry in a northern hardwood ecosystem. *Biogeochemistry*, 56(2): 215-238.  
897 DOI:10.1023/a:1013076609950
- 898 Fitzhugh, R.D. et al., 2003. Role of Soil Freezing Events in Interannual Patterns of Stream Chemistry at  
899 the Hubbard Brook Experimental Forest, New Hampshire. *Environ. Sci. Technol.*, 37(8): 1575-  
900 1580. DOI:10.1021/es026189r
- 901 Guo, L., Cai, Y., Belzile, C., Macdonald, R.W., 2012. Sources and export fluxes of inorganic and organic  
902 carbon and nutrient species from the seasonally ice-covered Yukon River. *Biogeochemistry*,  
903 107(1): 187-206.
- 904 Haei, M. et al., 2010. Cold winter soils enhance dissolved organic carbon concentrations in soil and  
905 stream water. *Geophys. Res. Lett.*, 37(8): L08501. DOI:10.1029/2010GL042821
- 906 Heidel, S., 1956. The progressive lag of sediment concentration with flood waves. *EOS, Trans. Am.*  
907 *Geophys. Union*, 37(1): 56-66.
- 908 Holmes, R.M. et al., 2008. Lability of DOC transported by Alaskan rivers to the Arctic Ocean. *Geophys.*  
909 *Res. Lett.*, 35, L03402. DOI:10.1029/2007GL032837

- Horsburgh, J.S., Jones, A.S., Stevens, D.K., Tarboton, D.G., Mesner, N.O., 2010. A sensor network for high frequency estimation of water quality constituent fluxes using surrogates. *Environ. Model. Softw.*, 25(9): 1031-1044. DOI:<http://dx.doi.org/10.1016/j.envsoft.2009.10.012>
- IPCC, 2014. *Climate Change 2014: Synthesis Report. Contribution of Working Groups I, II and III to the Fifth Assessment Report of the Intergovernmental Panel on Climate Change* [Core Writing Team, R.K. Pachauri and L.A. Meyer (eds.)]. IPCC, Geneva, Switzerland, 151 pp.
- Jones, A.S., Horsburgh, J.S., Mesner, N.O., Ryel, R.J., Stevens, D.K., 2012. Influence of Sampling Frequency on Estimation of Annual Total Phosphorus and Total Suspended Solids Loads<sup>1</sup>. *J. Am. Water Resour. Assoc.*, 48(6): 1258-1275. DOI:10.1111/j.1752-1688.2012.00684.x
- Jones, A.S., Stevens, D.K., Horsburgh, J.S., Mesner, N.O., 2011. Surrogate Measures for Providing High Frequency Estimates of Total Suspended Solids and Total Phosphorus Concentrations. *J. Am. Water Resour. Assoc.*, 47(2): 239-253. DOI:10.1111/j.1752-1688.2010.00505.x
- Kämäri, M. et al., 2015. River ice cover influence on sediment transportation at present and under projected hydroclimatic conditions. *Hydrol. Process.*, 29(22): 4738-4755. DOI:10.1002/hyp.10522
- Kämäri, M., Lotsari, E., Tattari, S., Koskiaho, J., 2016. River ice cover influence on water quality based on continuous monitoring and grab sampling data, 23rd IAHR International Symposium on Ice, Ann Arbor, Michigan.
- Kendall, C. et al., 1995. Tracing sources of nitrate in snowmelt runoff using the oxygen and nitrogen isotopic compositions of nitrate, *Biogeochemistry of Seasonally Snow-Covered Catchments* (Proceedings of a Boulder Symposium). IAHS Publ. no. 228, 1995, pp. 339-347.
- Kiirikki, M., 2018. Personal communication with the scan reseller in Finland. Luode Consulting Ltd. [www.luode.net](http://www.luode.net)
- Kortelainen, P., 1993. Content of total organic carbon in Finnish lakes and its relationship to catchment characteristics. *Can. J. Fish. Aquat. Sci.*, 50(7): 1477-1483.

- 934 Koskiaho, J., Tattari, S., Röman, E., 2015. Suspended solids and total phosphorus loads and their spatial  
935 differences in a lake-rich river basin as determined by automatic monitoring network. *Environ.*  
936 *Monit. Assess.*, 187(4): 187. DOI:10.1007/s10661-015-4397-6
- 937 Kotamäki, N. et al., 2009. Wireless in-situ Sensor Network for Agriculture and Water Monitoring on a  
938 River Basin Scale in Southern Finland: Evaluation from a Data User's Perspective. *Sensors*, 9(4):  
939 2862.
- 940 Lau, Y.L., Krishnappan, B.G., 1985. Sediment transport under ice cover. *J. Hydraul. Eng.*, 111(6): 934-  
941 950.
- 942 Laznik, M., Stålnacke, P., Grimvall, A., Wittgren, H.B., 1999. Riverine input of nutrients to the Gulf of  
943 Riga — temporal and spatial variation. *J. Mar. Syst.*, 23(1–3): 11-25.  
944 DOI:http://dx.doi.org/10.1016/S0924-7963(99)00048-2
- 945 Lepistö, A., Kortelainen, P., Mattsson, T., 2008. Increased organic C and N leaching in a northern boreal  
946 river basin in Finland. *Glob. Biogeochem. Cycles*, 22(GB3029): 1-10.  
947 DOI:10.1029/2007GB003175
- 948 Lloyd, C.E.M., Freer, J.E., Johnes, P.J., Coxon, G., Collins, A.L., 2016a. Discharge and nutrient  
949 uncertainty: implications for nutrient flux estimation in small streams. *Hydrol. Process.*, 30(1):  
950 135-152. DOI:10.1002/hyp.10574
- 951 Lloyd, C.E.M., Freer, J.E., Johnes, P.J., Collins, A.L., 2016b. Technical Note: Testing an improved index  
952 for analysing storm discharge–concentration hysteresis. *Hydrol. Earth Syst. Sci.*, 20(2): 625-632.  
953 DOI:10.5194/hess-20-625-2016
- 954 Lloyd, C.E.M., Freer, J.E., Johnes, P.J., Collins, A.L., 2016c. Using hysteresis analysis of high-resolution  
955 water quality monitoring data, including uncertainty, to infer controls on nutrient and sediment  
956 transfer in catchments. *Sci. Total Environ.*, 543: 388-404.  
957 DOI:http://dx.doi.org/10.1016/j.scitotenv.2015.11.028
- 958 Luterbacher, J., Dietrich, D., Xoplaki, E., Grosjean, M., Wanner, H., 2004. European seasonal and annual  
959 temperature variability, trends, and extremes since 1500. *Science*, 303(5663): 1499-1503.



- 960 Magnuson, J.J. et al., 2000. Historical Trends in Lake and River Ice Cover in the Northern Hemisphere.  
 961 Science, 289(5485): 1743-1746. DOI:10.1126/science.289.5485.1743
- 962 Mattsson, T., Kortelainen, P., Räike, A., 2005. Export of DOM from Boreal Catchments: Impacts of Land  
 963 Use Cover and Climate. Biogeochemistry, 76(2): 373-394. DOI:10.1007/s10533-005-6897-x
- 964 Mattsson, T., Kortelainen, P., Räike, A., Lepistö, A., Thomas, D.N., 2015. Spatial and temporal  
 965 variability of organic C and N concentrations and export from 30 boreal rivers induced by land  
 966 use and climate. Sci. Total Environ., 508(0): 145-154.  
 967 DOI:http://dx.doi.org/10.1016/j.scitotenv.2014.11.091
- 968 Matzner, E., Borken, W., 2008. Do freeze-thaw events enhance C and N losses from soils of different  
 969 ecosystems? A review. Eur. J. Soil Sci., 59(2): 274-284.
- 970 McDonald, D.M., Lamoureux, S.F., 2009. Hydroclimatic and channel snowpack controls over suspended  
 971 sediment and grain size transport in a High Arctic catchment. Earth Surf. Process. Landf., 34(3):  
 972 424-436. DOI:10.1002/esp.1751
- 973 Moatar, F., Abbott, B.W., Minaudo, C., Curie, F., Pinay, G., 2017. Elemental properties, hydrology, and  
 974 biology interact to shape concentration-discharge curves for carbon, nutrients, sediment, and  
 975 major ions. Water Resour. Res., 53(2): 1270-1287. DOI:doi:10.1002/2016WR019635
- 976 Muste, M., Braileanu, F., Ettema, R., 2000. Flow and sediment transport measurements in a simulated  
 977 ice-covered channel. Water Resour. Res., 36(9): 2711-2720. DOI:10.1029/2000WR900168
- 978 NADP, 2017. NADP Maps and Data, Underhill, Vermont. National Atmospheric Deposition Program,  
 979 NADP Program Office, Illinois State Water Survey, University of Illinois, Champaign, IL 6182,  
 980 <http://nadp.sws.uiuc.edu/data/>.
- 981 Ockenden, M.C. et al., 2016. Changing climate and nutrient transfers: Evidence from high temporal  
 982 resolution concentration-flow dynamics in headwater catchments, Sci. Total Environ., 548-549:  
 983 325-339. DOI:http://doi.org/10.1016/j.scitotenv.2015.12.086
- 984 O'Flynn, B. et al., 2010. Experiences and recommendations in deploying a real-time, water quality  
 985 monitoring system. Meas. Sci. Technol., 21(12), 124004.



- 986 Ohte, N. et al., 2004. Tracing sources of nitrate in snowmelt runoff using a high-resolution isotopic  
 987 technique. *Geophys. Res. Lett.*, 31, L21506. DOI:10.1029/2004GL020908
- 988 Olsson, T. et al., 2015. Impacts of climate change on temperature, precipitation and hydrology in Finland  
 989 – studies using bias corrected Regional Climate Model data. *Hydrol. Earth Syst. Sci.*, 19(7): 3217-  
 990 3238. DOI:10.5194/hess-19-3217-2015
- 991 Outram, F.N. et al., 2014. High-frequency monitoring of nitrogen and phosphorus response in three rural  
 992 catchments to the end of the 2011–2012 drought in England. *Hydrol. Earth Syst. Sci.*, 18(9): 3429-  
 993 3448. DOI:10.5194/hess-18-3429-2014
- 994 Palviainen, M., Lehtoranta, J., Ekholm, P., Ruoho-Airola, T., Kortelainen, P., 2015. Land Cover Controls  
 995 the Export of Terminal Electron Acceptors from Boreal Catchments. *Ecosystems*, 18(2): 343-358.  
 996 DOI:10.1007/s10021-014-9832-y
- 997 Pellerin, B.A. et al., 2012. Taking the pulse of snowmelt: in situ sensors reveal seasonal, event and  
 998 diurnal patterns of nitrate and dissolved organic matter variability in an upland forest stream.  
 999 *Biogeochemistry*, 108(1): 183-198. DOI:10.1007/s10533-011-9589-8
- 1000 Pirinen, P. et al., 2012. Climatological statistics of Finland 1981–2010. Reports 2012:1. Finnish  
 1001 Meteorological Institute, Helsinki, Finland.
- 1002 Prowse, T. et al., 2011. Past and Future Changes in Arctic Lake and River Ice. *Ambio*, 40(1): 53-62.  
 1003 DOI:10.1007/s13280-011-0216-7
- 1004 Puustinen, M., Tattari, S., Koskiahho, J., Linjama, J., 2007. Influence of seasonal and annual hydrological  
 1005 variations on erosion and phosphorus transport from arable areas in Finland. *Soil Tillage Res.*,  
 1006 93(1): 44-55. DOI:10.1016/j.still.2006.03.011
- 1007 Qiao, H. et al., 2017. Snowpack enhanced dissolved organic carbon export during a variety of hydrologic  
 1008 of events in an agricultural landscape, Midwestern USA. *Agric. For. Meteorol.*, 246: 31-41.
- 1009 Räike, A., Kortelainen, P., Mattsson, T., Thomas, D.N., 2012. 36 year trends in dissolved organic carbon  
 1010 export from Finnish rivers to the Baltic Sea. *Sci. Total Environ.*, 435–436: 188-201.  
 1011 DOI:http://dx.doi.org/10.1016/j.scitotenv.2012.06.111

- 1012 Ramos, T.B. et al., 2015. Sediment and nutrient dynamics during storm events in the Enxoé temporary  
1013 river, southern Portugal. CATENA, 127: 177-190.  
1014 DOI:<http://dx.doi.org/10.1016/j.catena.2015.01.001>
- 1015 Randall, G.W., Mulla, D.J., 2001. Nitrate nitrogen in surface waters as influenced by climatic conditions  
1016 and agricultural practices. J. Environ. Qual., 30(2): 337-344.
- 1017 Rankinen, K. et al., 2013. Climate change adaptation in arable land use, and impact on nitrogen load at  
1018 catchment scale in northern agriculture. Agric. Food Sci., 22(3): 342-355.
- 1019 Rosberg, J., Arheimer, B., 2007. Modelling climate change impact on phosphorus load in Swedish rivers,  
1020 Water Quality and Sediment Behaviour of the Future: Predictions for the 21st Century  
1021 (Proceedings of Symposium HS2005 at IUGG2007, Perugia). IAHS Publ. 314, 2007.
- 1022 Ruoho-Airola, T., Hatakka, T., Kyllönen, K., Makkonen, U., Porvari, P., 2014. Temporal trends in the  
1023 bulk deposition and atmospheric concentration of acidifying compounds and trace elements in the  
1024 Finnish Integrated Monitoring catchment Valkea-Kotinen during 1988-2011. Boreal Env. Res., 19  
1025 (suppl. A): 31-46.
- 1026 Ruosteenoja, K., Jylhä, K., Kämäräinen, M., 2016. Climate Projections for Finland Under the RCP  
1027 Forcing Scenarios. Geophysica, 51(1/2): 17-50.
- 1028 Ruosteenoja, K., Tuomenvirta, H., Jylhä, K., 2007. GCM-based regional temperature and precipitation  
1029 change estimates for Europe under four SRES scenarios applying a super-ensemble pattern-  
1030 scaling method. Clim. Chang., 81(1): 193-208. DOI:10.1007/s10584-006-9222-3
- 1031 Scholefield, D. et al., 2005. Concerted diurnal patterns in riverine nutrient concentrations and physical  
1032 conditions. Sci. Total Environ., 344(1-3): 201-210.  
1033 DOI:<http://dx.doi.org/10.1016/j.scitotenv.2005.02.014>
- 1034 Scrimgeour, G.J., Prowse, T.D., Culp, J.M., Chambers, P.A., 1994. Ecological effects of river ice break-  
1035 up: a review and perspective. Freshwater Biol., 32(2): 261-275. DOI:10.1111/j.1365-  
1036 2427.1994.tb01125.x

- Sebestyen, S.D. et al., 2008. Sources, transformations, and hydrological processes that control stream nitrate and dissolved organic matter concentrations during snowmelt in an upland forest. *Water Resour. Res.*, 44, W12410. DOI:10.1029/2008WR006983
- Shakibaeinia, A., Dibike, Y.B., Kashyap, S., Prowse, T.D., Droppo, I.G., 2017. A numerical framework for modelling sediment and chemical constituents transport in the Lower Athabasca River. *J. Soils Sediments*, 17(4): 1140-1159. DOI:10.1007/s11368-016-1601-4
- Shibata, H., Hasegawa, Y., Watanabe, T., Fukuzawa, K., 2013. Impact of snowpack decrease on net nitrogen mineralization and nitrification in forest soil of northern Japan. *Biogeochemistry*, 116(1): 69-82. DOI:10.1007/s10533-013-9882-9
- Spencer, R.G.M. et al., 2007. Diurnal variability in riverine dissolved organic matter composition determined by in situ optical measurement in the San Joaquin River (California, USA). *Hydrol. Process.*, 21(23): 3181-3189. DOI:10.1002/hyp.6887
- Strohmeier, S. et al., 2013. Concentrations and fluxes of dissolved organic carbon in runoff from a forested catchment: insights from high frequency measurements. *Biogeosciences*, 10(2): 905-916. DOI:10.5194/bg-10-905-2013
- Su, J.J. et al., 2011. Effects of snowmelt on phosphorus and sediment losses from agricultural watersheds in Eastern Canada. *Agric. Water Manage.*, 98(5): 867-876. DOI:10.1016/j.agwat.2010.12.013
- SYKE, 2017. Open data, Finnish Environment Insitute (the web service is mainly available only in Finnish language), [http://www.syke.fi/en-US/Open\\_information](http://www.syke.fi/en-US/Open_information), (Accessed 28/5 2018).
- Tananaev, N.I., Debolskiy, M.V., 2014. Turbidity observations in sediment flux studies: Examples from Russian rivers in cold environments. *Geomorphology*, 218: 63-71. DOI:<http://doi.org/10.1016/j.geomorph.2013.09.031>
- Taylor, C.R., Hook, P.B., Stein, O.R., Zabinski, C.A., 2011. Seasonal effects of 19 plant species on COD removal in subsurface treatment wetland microcosms. *Ecol. Eng.*, 37(5): 703-710. DOI:<https://doi.org/10.1016/j.ecoleng.2010.05.007>

- Valkama, P., Ruth, O., 2017. Impact of calculation method, sampling frequency and hysteresis on suspended solids and total phosphorus load estimations in cold climate. *Hydrol. Res.*, 48(6): 1594-1610. DOI:10.2166/nh.2017.199
- van den Broeke, J., Langergraber, G., Weingartner, A., 2006. On-line and in-situ UV/vis spectroscopy for multi-parameter measurements: a brief review. *Spectroscopy Europe*, 18(4): 15-18.
- Vaughan, M.C. et al., 2017. High-frequency dissolved organic carbon and nitrate measurements reveal differences in storm hysteresis and loading in relation to land cover and seasonality. *Water Resour. Res.*, 53(7): 5345-5363.
- Veijalainen, N., Lotsari, E., Alho, P., Vehviläinen, B., Käyhkö, J., 2010. National scale assessment of climate change impacts on flooding in Finland. *J. Hydrol.*, 391(3-4): 333-350. DOI:10.1016/j.jhydrol.2010.07.035
- Vuorenmaa, J., Rekolainen, S., Lepistö, A., Kenttämies, K., Kauppila, P., 2002. Losses of Nitrogen and Phosphorus from Agricultural and Forest Areas in Finland during the 1980s and 1990s. *Environ. Monit. Assess.*, 76(2): 213-248. DOI:10.1023/a:1015584014417
- Williams, G.P., 1989. Sediment concentration versus water discharge during single hydrologic events in rivers. *J. Hydrol.*, 111(1-4): 89-106.
- Williams, M.R. et al., 2015. Uncertainty in nutrient loads from tile-drained landscapes: Effect of sampling frequency, calculation algorithm, and compositing strategy. *J. Hydrol.*, 530: 306-316. DOI:http://dx.doi.org/10.1016/j.jhydrol.2015.09.060
- Worrall, F., Howden, N.J.K., Burt, T.P., 2013. Assessment of sample frequency bias and precision in fluvial flux calculations – An improved low bias estimation method. *J. Hydrol.*, 503: 101-110. DOI:http://doi.org/10.1016/j.jhydrol.2013.08.048
- Worrall, F., Howden, N.J.K., Burt, T.P., 2015. Understanding the diurnal cycle in fluvial dissolved organic carbon – The interplay of in-stream residence time, day length and organic matter turnover. *J. Hydrol.*, 523: 830-838. DOI:http://dx.doi.org/10.1016/j.jhydrol.2015.01.075

- 1087 Zhao, Q., Chang, D., Wang, K., Huang, J., 2017. Patterns of nitrogen export from a seasonal freezing  
1088 agricultural watershed during the thawing period. *Sci. Total Environ.*, 599–600: 442-450.  
1089 DOI:<https://doi.org/10.1016/j.scitotenv.2017.04.174>
- 1090 Øygarden, L. et al., 2014. Climate change and the potential effects on runoff and nitrogen losses in the  
1091 Nordic–Baltic region. *Agric. Ecosyst. Environ.* 198: 114-126.  
1092 DOI:<https://doi.org/10.1016/j.agee.2014.06.025>

1093

1094 Fig. 1. Location of the study area and monitoring sites. The in-situ monitoring site 1 drains 73% of the  
1095 whole Vantaa River catchment.

1096

1097 Fig. 2. Discharge magnitude during grab sampling and exceedance frequency of the discharge.

1098

1099 Fig. 3. Water quality variation in the Vantaa River during 2010–2014. Precipitation and air temperature  
1100 are from the Helsinki airport (Finnish Meteorological Institute, open data portal).

1101

1102 Fig. 4. The monthly flow-weighted average concentrations of suspended solids, nitrate-nitrogen ( $\text{NO}_3\text{-N}$ )  
1103 and chemical oxygen demand (COD), as well as monthly average temperatures (average of five stations  
1104 within the basin, Finnish Meteorological Institute, open data portal) and discharge.

1105

1106 Fig. 5. Daily mean turbidity values, nitrate-nitrogen ( $\text{NO}_3\text{-N}$ ) and chemical oxygen demand (COD)  
1107 concentrations during 315 summer days, 215 autumn days and 286 ice covered river days versus  
1108 discharges. The days with mean discharge below  $10 \text{ m}^3 \text{ s}^{-1}$  were selected for the figure from the period  
1109 2010–2014.

1110

1111 Fig. 6. Discharge variation and hysteresis indices during storms for turbidity, nitrate-nitrogen ( $\text{NO}_3\text{-N}$ )  
1112 and chemical oxygen demand (COD). Some of the storms are indicated with a running number. The ice  
1113 cover periods are shaded with grey. The snow water equivalent (SWE) represents the average of three  
1114 snow courses within the Vantaa River basin.

1115

1116 Fig. 7. A), Total suspended solids, nitrate-nitrogen ( $\text{NO}_3\text{-N}$ ) and organic matter cumulative loads  
1117 determined based on chemical oxygen demand (COD) from November to the end of May. Cumulative  
1118 discharge is denoted with the lines combined with circles. The horizontal bars in the pane A indicate  
1119 flow-weighted mean concentrations from November to the end of May. Note that COD measurement  
1120 started first 3 December 2010. B) Cumulative riverine loads versus cumulative discharge during 60 days  
1121 of freshet periods 2011–2014 starting from the river ice clearance date.

1122

1123 Fig. 8. Concentration-discharge (C-Q) response of turbidity, nitrate-nitrogen ( $\text{NO}_3\text{-N}$ ) and chemical  
1124 oxygen demand (COD) during 91 storm events illustrated in the flushing index ( $\Delta C$ ) versus hysteresis  
1125 index (HI) unity plane. The dotted lines indicate the threshold of the appearance of hysteresis.

1126

1127 Fig. 9. Turbidity,  $\text{NO}_3\text{-N}$  and COD variation during winter-spring time storms 2011–2014.

1128

1129 Fig. 10. Turbidity, NO<sub>3</sub>-N and COD response to spring storm events during the years 2011–2014.

1130

ACCEPTED MANUSCRIPT



Table 1. Summary of relevant research conducted to study seasonal and event scale concentration-discharge (C-Q) pattern in rivers draining mixed or agricultural land use catchments located in cold and temperate region in Northern Hemisphere. In the 'Key results' column is identified results related to the aims of the present paper: (1) seasonality in turbidity, total suspended solids (TSS) suspended solids (SS), nitrate-nitrogen ( $\text{NO}_3\text{-N}$ ), chemical oxygen demand (COD) or dissolved organic carbon (DOC) level variation; (2) event scale C-Q analysis results: key drivers of C-Q variation and/or main hysteresis pattern where clockwise hysteresis combined with concentration pattern indicate transport-limited system and anti-clockwise hysteresis together with dilution pattern indicate source limited system; (3) snow water equivalent (SWE), snow depth, ground frost depth and snowmelt variation influences on hysteresis, solute concentration or loads. Studies contributing into at least two of the three 'Key results' topics were included into the table.

Study	Location/ catchment size/Q/annual mean temperature	Characteristic land use/main soil type	Measured parameter/sampling interval, monitoring period	Key results
1. Lloyd et al. (2016c)	Hampshire Avon, UK/ 5 and 50 $\text{km}^2$ /0.06-0.34 $\text{m}^3\text{s}^{-1}$ /9°C	Two catchments, mixed livestock, arable farming/chalk or clay	$\text{NO}_3\text{-N}$ , TP, turbidity/hourly, 24 months	<ol style="list-style-type: none"> <li>1. No strong seasonal changes in <math>\text{NO}_3\text{-N}</math> concentration or seasonality in <math>\text{NO}_3\text{-N}</math> hysteresis, but dry/wet antecedent periods influenced hysteresis</li> <li>2. Clockwise <math>\text{NO}_3\text{-N}</math> hysteresis and dilution dominated in a groundwater dominated chalk catchment Highly varying turbidity hysteresis in a groundwater dominated site and mainly clockwise turbidity hysteresis in a clayed surface-water dominated headwater catchment.</li> <li>3. N/A</li> </ol>
2. Blaen et al. (2017)	The Wood Brook, UK/3.1 $\text{km}^2$ /mean 12.7 L $\text{s}^{-1}$ /9°C	Mixed, arable farming, woodland, tile drains/sandy clay, till	$\text{NO}_3\text{-N}$ , DOC/hourly, 8 months	<ol style="list-style-type: none"> <li>1. The highest DOC concentration in late August and decline through the autumn, no seasonality in <math>\text{NO}_3\text{-N}</math> concentrations</li> <li>2. Clockwise and anticlockwise hysteresis and both flushing and dilution of <math>\text{NO}_3\text{-N}</math> and DOC during storm events. <math>\text{NO}_3\text{-N}</math> concentrations were typically diluted on the rising limbs of storm hydrographs, whereas patterns in DOC concentrations generally exhibited flushing behavior through storm events.</li> <li>3. N/A</li> </ol>
3. Valkama and Ruth (2017)	Lepsämäenjoki River in the Vantaa River catchment and Lukupuro River, Finland/8-23 $\text{km}^2$ /-5.3°C	Agriculture/clay, till and rocky areas	Turbidity, TSS, TP/hourly, 12 months	<ol style="list-style-type: none"> <li>1. The highest TSS concentrations in spring thaw and autumn. No clear seasonality in hysteresis direction</li> <li>2. TSS and TP predominantly clockwise hysteresis</li> <li>3. Anti-clockwise TP hysteresis during snowmelt due to frozen surface of the fields</li> </ol>
4. Zhao et al. (2017)	Heidingzi watershed, NE China/75 $\text{km}^2$ /-4.8°C	Mixed, agriculture, forest/-	$\text{NO}_3\text{-N}$ /daily, three thawing periods (2004-06)	<ol style="list-style-type: none"> <li>1. N/A</li> <li>2. The highest <math>\text{NO}_3\text{-N}</math> concentrations at the beginning of snowmelt</li> <li>3. Flushing effect and solute concentrations were controlled by soil frost status, soil ice content and thaw depth during snowmelt. Early snow melt quickly saturated thawed soil and introduced flushing effect</li> </ol>
5. Bieroza and Heathwaite (2015)	River Leith, UK/54 $\text{km}^2$ /0.1–37.8 $\text{m}^3\text{s}^{-1}$ depending on storm event/5°C mean at the winter and 14°C mean at the summer (cf. their Table 4)	Grassland, woodland, arable land/ Carboniferous Limestone, Penrith Permo-Triassic Sandstone, glacial till deposits	Turbidity, P/hourly water samples, 24 months	<ol style="list-style-type: none"> <li>1. Seasonally varying discharge and temperature control turbidity hysteresis loop direction, but rainfall controls the magnitude.</li> <li>2. Similar frequency of anti-clockwise and clockwise hysteresis. The hysteresis direction correlated with discharge</li> <li>3. N/A</li> </ol>
6. Guo et al. (2012)	Yukon River, Canada, Alaska/ 202 $\text{km}^2$ /range 1293–19858 $\text{m}^3\text{s}^{-1}$ /water temp range - 0.18–19 °C	Subarctic/arctic catchment, where frozen period has been projected to shorten due to climatic change.	DOC, N, TSS/ monthly for c. 14 months	<ol style="list-style-type: none"> <li>1. Seasonal differences in DOC and inorganic N concentrations were great, as highest values occurred during spring freshet and lowest ice-covered winter conditions.</li> <li>2. N/A</li> <li>3. Dominant sources of all organic carbon and nutrient species were from</li> </ol>

7. Cerro et al. 2014	Alegria watershed, Spain/113/53 km <sup>2</sup> / range 0.1-19 m <sup>3</sup> s <sup>-1</sup> /sub-zero in winter, >25°C in summer	Agriculture 75%, forest 25%/ clays and silts with sand and gravel	TSS, NO <sub>3</sub> -N, DOC/10 min, 24 months	<ol style="list-style-type: none"> <li>1. Low NO<sub>3</sub>-N concentrations during summer</li> <li>2. Particulate TSS experienced clockwise hysteresis and dissolved (DOC, NO<sub>3</sub>-N) matter anti-clockwise hysteresis, flushing of suspended sediments and DOC, dilution common for NO<sub>3</sub>-N</li> <li>3. Snowmelt storm diluted NO<sub>3</sub>-N, slightly flushed DOC, intensively flushed suspended sediments and introduced a large suspended sediment load.</li> </ol>
8. Vaughan et al. 2017	3 sites in the Lake Champlain Basin, Vermont U.S./11-95 km <sup>2</sup> / /4.2-6.7°C	Three watersheds: agricultural, urban, forested/loam, clay, mixed northern hardwoods and conifer	NO <sub>3</sub> -N, DOC/15 min, June 2014 – Dec. 2015 excluding winter	<ol style="list-style-type: none"> <li>1. They found no seasonal pattern in NO<sub>3</sub>-N/DOC hysteresis or flushing index</li> <li>2. Anti-clockwise DOC hysteresis at all sites, predominantly clockwise NO<sub>3</sub>-N hysteresis for urban and forested sites but anti-clockwise for agricultural site. NO<sub>3</sub>-N hysteresis index had higher variability than DOC hysteresis index. Flushing of DOC, NO<sub>3</sub>-N dilution at urban and forest sites, dilution or flushing of NO<sub>3</sub>-N from agricultural site.</li> <li>3. The ratio of storm nitrate yield to water yield was low in the forested site and highest during snowmelt events</li> </ol>
9. Qiao et al. 2017	Chippewa River watershed Michigan USA/1037 km <sup>2</sup> /7.2 m <sup>3</sup> s <sup>-1</sup> /-	Agriculture 45%, forest 40%	DOC/1-2 h interval auto-sampling/ spring and autumn 2013 – 2015	<ol style="list-style-type: none"> <li>1. High DOC concentrations in the spring. Greater storm DOC flux in the spring than in the autumn</li> <li>2. DOC peak preceded spring storm Qpeak and lagged behind autumn Qpeak</li> <li>3. Snowpack likely catalyzed the transformation of DOC from agricultural residues, which led to intensive DOC flushing during snowmelt</li> </ol>
10. This study	Vantaa River, Finland/1680 km <sup>2</sup> /mean 11 m <sup>3</sup> s <sup>-1</sup> /5.3°C	Mixed, agriculture 27%, forest 60%/moraine, clay soils, mixed northern hardwoods and conifer	Turbidity, TSS, NO <sub>3</sub> -N, COD/hourly, 50 months	<ol style="list-style-type: none"> <li>1. TSS and NO<sub>3</sub>-N concentrations the highest in the spring thaw or autumn, COD concentrations the highest in the autumn</li> <li>2. Predominantly anti-clockwise hysteresis of turbidity, NO<sub>3</sub>-N and COD and flushing of suspended solids and organic matter. Solute concentrations correlated with the storm discharges. NO<sub>3</sub>-N flushing turns to dilution pattern during consecutive storms</li> <li>3. Large snowmelt storms resulted clockwise hysteresis of turbidity and NO<sub>3</sub>-N but anti-clockwise COD hysteresis. Thick snow pack and lack of ground frost promoted spring storm related flushing of NO<sub>3</sub>-N whereas ground frost during winter was a likely influencing factor in an event base dilution of NO<sub>3</sub>-N during spring storms 2014.</li> </ol>

1142

1143

1144

1145 Table 2. Estimated ice cover periods of the Vantaa River and measured snow depth in the basin (Finnish  
 1146 Meteorological Institute).

Winter	Certain ice cover in the Vantaa River	Ice cover period length (days)	Snow depth (cm) in the Vantaa River basin		
			15 <sup>th</sup> Feb.	15 <sup>th</sup> March	15 <sup>th</sup> April
2010–11	15/12/ – 01/04	108	50–75	50–75	<1–10
2011–12	01/02 – 13/03	42	25–50	25–50	1–25
2012–13	13/12 – 10/04	119	25–75	25–75	10–50
2013–14	17/01/ – 04/03	47	1–10	1–10	<1

1147

1148

1149 Table 3. In-situ measurement conversion equations for turbidity and total suspended solids (TSS), nitrate-  
 1150 N (NO<sub>3</sub>-N), and chemical oxygen demand (COD) concentrations as determined primary measured  
 1151 turbidity, NO<sub>3</sub>-N and DOC values. n = number of water samples used in the formation of conversion  
 1152 equations.

Measured variable	Measurement model/ Conversion equation	Coefficient of determination, R <sup>2</sup>	x	Standard error of the estimate, S <sub>est</sub>	n
Turbidity	c = 1.80x+1.72	0.93	in-situ primary turbidity	10.2 FTU	21
TSS concentration	c = 1.43x-3.52	0.88	in-situ primary turbidity	10.8 mg L <sup>-1</sup>	21
NO <sub>3</sub> -N concentration	c = 0.61x	0.85	in-situ primary NO <sub>3</sub> -N	0.3 mg L <sup>-1</sup>	20
COD concentration	c = 0.53x+4.51	0.83	in-situ primary DOC	2.8 mg L <sup>-1</sup>	15

1153

1154

1155

1156 Table 4. Goodness of fit statistics between calibrated in-situ measurements from site 1 and laboratory  
 1157 measurements based on grab samples (Lab) from sites 1 and 2.

Statistic	Data source	Turbidity (FTU)	NO <sub>3</sub> -N (mg L <sup>-1</sup> )	COD (mg L <sup>-1</sup> )
Mean	In situ / Lab, site 1	42.3 / 42.3	2.0 / 2.0	16.0 / 16.6
	In situ / Lab, site 2	46.3 / 45.5	1.8 / 1.9	15.1 / 13.6
Estimated standard deviation, $\sigma_{n-1}$	In situ / Lab, site 1	35.8 / 37.1	0.7 / 0.8	5.9 / 6.4
	In situ / Lab, site 2	59.1 / 65.0	0.7 / 0.9	5.8 / 4.6
Number of grab sample and in-situ data pairs	Site 1 / Site 2	21 / 46	20 / 45	15 / 44
Mean absolute error	Site 1 / Site 2	6.2 / 8.3	0.2 / 0.2	2.1 / 2.0
Median error	Site 1 / Site 2	3.0 / 4.4	0.1 / 0.1	1.5 / 1.3
Mean percentage error (%)	Site 1 / Site 2	20% / 37%	13% / 13%	12% / 15%
Median error (%)	Site 1 / Site 2	13% / 19%	6% / 9%	11% / 9%
Standard error of the estimate, $S_{est}$	Site 1 / Site 2	10.2 / 13.1	0.3 / 0.3	2.8 / 3.0
Pearson's correlation coefficient <sup>a</sup>	Site 1 / Site 2	0.96 / 0.98	0.94 / 0.95	0.91 / 0.85

1158 <sup>a</sup>correlation is significant at the 0.01 level (2-tailed)

1159

1160 Table 5. Loads based on hourly water quality and discharge monitoring during hydrological years starting  
 1161 1 November. The loads are interpolated 20/12/2012–07/01/2013 and <sup>\*)</sup>COD data is missing from  
 1162 November 2010. Precipitation from Helsinki Airport (Finnish Meteorological Institute, FMI open data  
 1163 portal)

Hydrological year	$Q_{\text{mean}}$ ( $\text{m}^3 \text{s}^{-1}$ )	P ( $\text{mm a}^{-1}$ )	Load (tn)			Flow-weighted mean concentration ( $\text{mg L}^{-1}$ )		
			TSS	$\text{NO}_3\text{-N}$	COD	TSS	$\text{NO}_3\text{-N}$	COD
2010–2011	8	600	14 500	736	3 940 <sup>*)</sup>	59	3.0	16 <sup>*)</sup>
2011–2012	19	950	41 360	1 315	13 170	68	2.2	22
2012–2013	9	510	18 120	595	5 510	62	2.0	19
2013–2014	8	640	15 980	588	5 320	60	2.2	20
Mean	11	670	22 490	808	6 980	64	2.3	20

1166 Table 6. Storm characteristics between seasons, and during the entire study period. Standard deviation  
 1167 (*SD*) is given in brackets besides the average values.

	Autumn storms	All winter storms including ice-covered cases	Ice-covered river	Spring storms	Summer storms	All storms 2010–2014
Number of storms	42	17	10	15	17	91
HI mean turbidity	-0.16 (0.30)	-0.14 (0.27)	-0.16 (0.23)	0.01 (0.29)	-0.17 (0.15)	-0.13 (0.27)
HI mean NO <sub>3</sub> -N	-0.21 (0.30)	0.02 (0.29)	0.02 (0.28)	-0.08 (0.40)	-0.28 (0.26)	-0.16 (0.32)
HI mean COD	-0.30 (0.29)	-0.31 (0.40)	-0.36 (0.40)	-0.24 (0.38)	-0.29 (0.42)	-0.29 (0.35)
Average storm duration Turbidity ( <i>SD</i> ), (h)	132 (70)	144 (82)	130 (70)	294 (283)	205 (57)	174 (144)
Average storm duration NO <sub>3</sub> -N ( <i>SD</i> ), (h)	134 (71)	179 (142)	130 (70)	320 (286)	241 (107)	192 (163)
Average storm duration COD ( <i>SD</i> ), (h)	136 (73)	151 (85)	130 (70)	323 (305)	266 (132)	195 (169)
Average Q <sub>peak</sub> ( <i>SD</i> ), (m <sup>3</sup> s <sup>-1</sup> )	31 (21)	14 (14)	7 (6)	40 (40)	7 (5)	25 (25)
Average Turbidity ( <i>SD</i> ), (FTU)	84 (36)	33 (21)	23 (14)	62 (26)	34 (14)	61 (37)
Average NO <sub>3</sub> -N ( <i>SD</i> ), (mg L <sup>-1</sup> )	2.6 (0.8)	1.8 (0.3)	1.7 (0.2)	1.9 (0.3)	1.5 (0.3)	2.1 (0.7)
Average COD ( <i>SD</i> ), (mg L <sup>-1</sup> )	22.1 (5.7)	14.3 (3.9)	11.7 (1.6)	17.2 (2.4)	11.9 (2.4)	17.8 (6.1)
Turbidity average range ( <i>SD</i> ), (FTU)	113 (83)	34 (31)	26 (25)	100 (64) <sup>a</sup>	60 (35)	83 (72)
NO <sub>3</sub> -N average range ( <i>SD</i> ), (mg L <sup>-1</sup> )	1.0 (0.7)	0.4 (0.4)	0.3 (0.2)	1.3 (1.1) <sup>a</sup>	0.8 (0.4)	0.8 (0.7)
COD average range ( <i>SD</i> ), (mg L <sup>-1</sup> )	8.2 (5.7)	2.3 (3.2)	1.0 (1.1)	5.9 (3.1) <sup>a</sup>	3.7 (3.6)	5.6 (5.1)
ΔC average Turbidity ( <i>SD</i> ), (%)	46 (32)	25 (25)	22 (25)	44 (35)	25 (35)	38 (34)
ΔC average NO <sub>3</sub> -N ( <i>SD</i> ), (%)	-2 (14)	1 (15)	-2 (10)	5 (21)	5 (15)	1 (16)
ΔC average COD ( <i>SD</i> ), (%)	16 (17)	4 (10)	2 (4)	14 (15)	6 (14)	12 (16)

1168 <sup>a</sup>3 minor storms due to diurnal discharge fluctuation from spring 2014 (numbered 74–76) are not included

1169

1170



1171 Table 7. Spearman's rho nonparametric correlation analysis of the storms during 2010–2014. Only  
1172 significant correlations are shown.

Pairwise correlation pairs		Autumn storms (n=39–42)	Winter storms (n=17)	Spring storms (n=15)	Summer storms (n=17)	All storms 2010–2014 (n=88–91)
Q <sub>peak</sub> vs.	Turbidity mean	.84 <sup>a</sup>	.87 <sup>a</sup>	.83 <sup>a</sup>	.80 <sup>a</sup>	.87 <sup>a</sup>
Q <sub>peak</sub> vs.	NO <sub>3</sub> -N mean			.70 <sup>a</sup>	.73 <sup>a</sup>	.61 <sup>a</sup>
Q <sub>peak</sub> vs.	COD mean	.83 <sup>a</sup>	.90 <sup>a</sup>	.74 <sup>a</sup>	.98 <sup>a</sup>	.88 <sup>a</sup>
Q <sub>range</sub> vs.	Turbidity mean	.61 <sup>a</sup>	.91 <sup>a</sup>	.79 <sup>a</sup>	.79 <sup>a</sup>	.79 <sup>a</sup>
Q <sub>range</sub> vs.	NO <sub>3</sub> -N mean			.65 <sup>a</sup>	.75 <sup>a</sup>	.55 <sup>a</sup>
Q <sub>range</sub> vs.	COD mean	.51 <sup>a</sup>	.90 <sup>a</sup>	.68 <sup>a</sup>	.93 <sup>a</sup>	.75 <sup>a</sup>
Q <sub>peak</sub> vs.	TSS load	.95 <sup>a</sup>	.92 <sup>a</sup>	.95 <sup>a</sup>	.94 <sup>a</sup>	.96 <sup>a</sup>
Q <sub>peak</sub> vs.	NO <sub>3</sub> -N load	.85 <sup>a</sup>	.92 <sup>a</sup>	.96 <sup>a</sup>	.86 <sup>a</sup>	.93 <sup>a</sup>
Q <sub>peak</sub> vs.	COD load	.93 <sup>a</sup>	.96 <sup>a</sup>	.94 <sup>a</sup>	.87 <sup>a</sup>	.95 <sup>a</sup>
Q <sub>peak</sub> vs.	Turbidity range	.64 <sup>a</sup>	.71 <sup>a</sup>	.90 <sup>a</sup>	.66 <sup>a</sup>	.71 <sup>a</sup>
Q <sub>peak</sub> vs.	NO <sub>3</sub> -N range		.57 <sup>b</sup>	.76 <sup>a</sup>	.57 <sup>b</sup>	.46 <sup>a</sup>
Q <sub>peak</sub> vs.	COD range		.83 <sup>a</sup>	.83 <sup>a</sup>	.74 <sup>a</sup>	.66 <sup>a</sup>
Q <sub>peak</sub> vs.	Turbidity lag	-.71 <sup>a</sup>				-.36 <sup>a</sup>
Q <sub>peak</sub> vs.	NO <sub>3</sub> -N lag	-.42 <sup>a</sup>		-.56 <sup>b</sup>		-.32 <sup>a</sup>
Q <sub>peak</sub> vs.	COD lag	-.55 <sup>a</sup>				
Q <sub>peak</sub> vs.	HI turbidity	.65 <sup>a</sup>			-.56 <sup>b</sup>	.31 <sup>a</sup>
Q <sub>peak</sub> vs.	HI NO <sub>3</sub> -N					
Q <sub>peak</sub> vs.	HI COD				-.72 <sup>a</sup>	
HI turb. vs.	HI NO <sub>3</sub> -N	.38 <sup>b</sup>				.28 <sup>a</sup>
HI turb. vs.	HI COD	.76 <sup>a</sup>	.73 <sup>a</sup>	.75 <sup>a</sup>		.71 <sup>a</sup>
HI NO <sub>3</sub> -N vs.	HI COD					
HI turb. vs.	Range turb.				-.55 <sup>b</sup>	
HI NO <sub>3</sub> -N vs.	Range NO <sub>3</sub> -N	-.42 <sup>a</sup>				-.38 <sup>a</sup>
HI COD vs.	Range COD	-.32 <sup>b</sup>			-.55 <sup>b</sup>	
Range turb. vs.	Range NO <sub>3</sub> -N	.53 <sup>a</sup>	.71 <sup>a</sup>	.84 <sup>a</sup>		.72 <sup>a</sup>
Range turb. vs.	Range COD	.84 <sup>a</sup>	.84 <sup>a</sup>	.92 <sup>a</sup>	.75 <sup>a</sup>	.89 <sup>a</sup>
Turb. mean vs.	NO <sub>3</sub> -N mean					.62 <sup>a</sup>
Turb. mean vs.	COD mean	.83 <sup>a</sup>	.83 <sup>a</sup>	.88 <sup>a</sup>	.84 <sup>a</sup>	.93 <sup>a</sup>

1173 <sup>a</sup>correlation is significant at the 0.01 level (2-tailed), <sup>b</sup>correlation is significant at the 0.05 level

1174

Figure1

ACCEPTED MANUSCRIPT

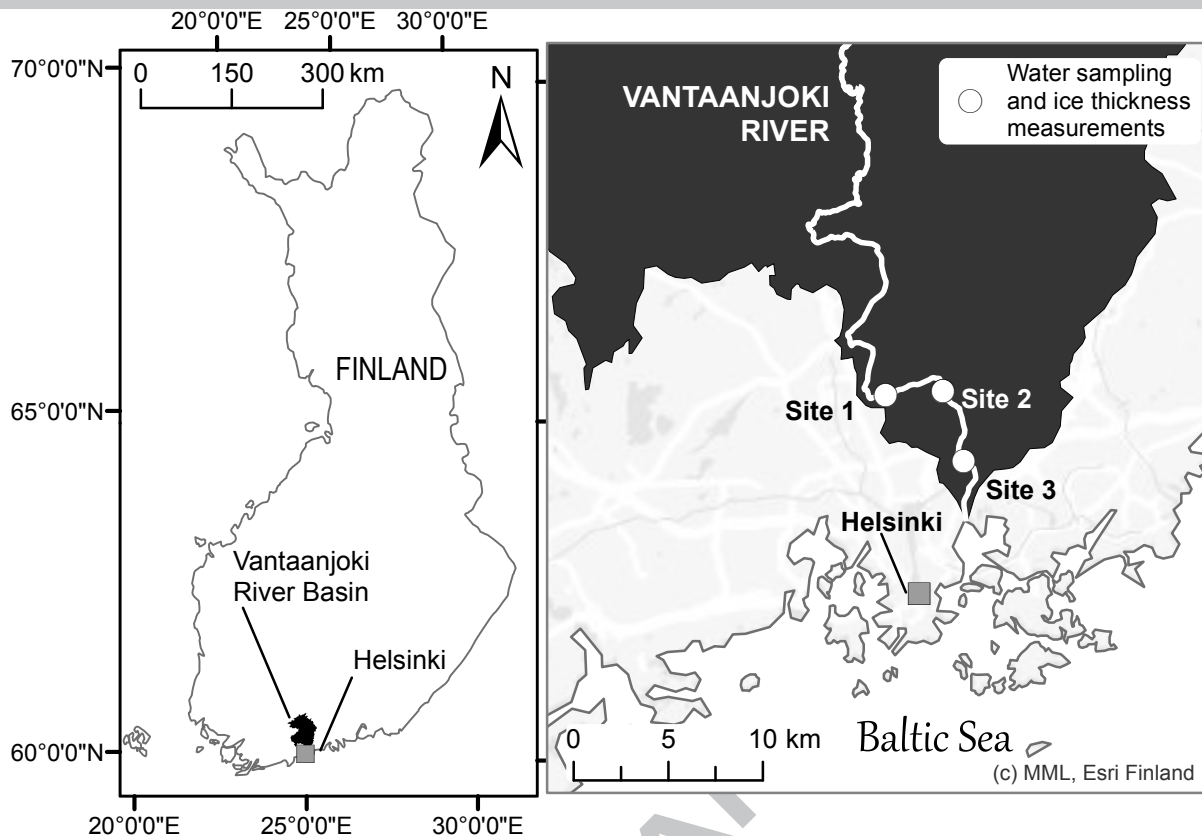


Figure2

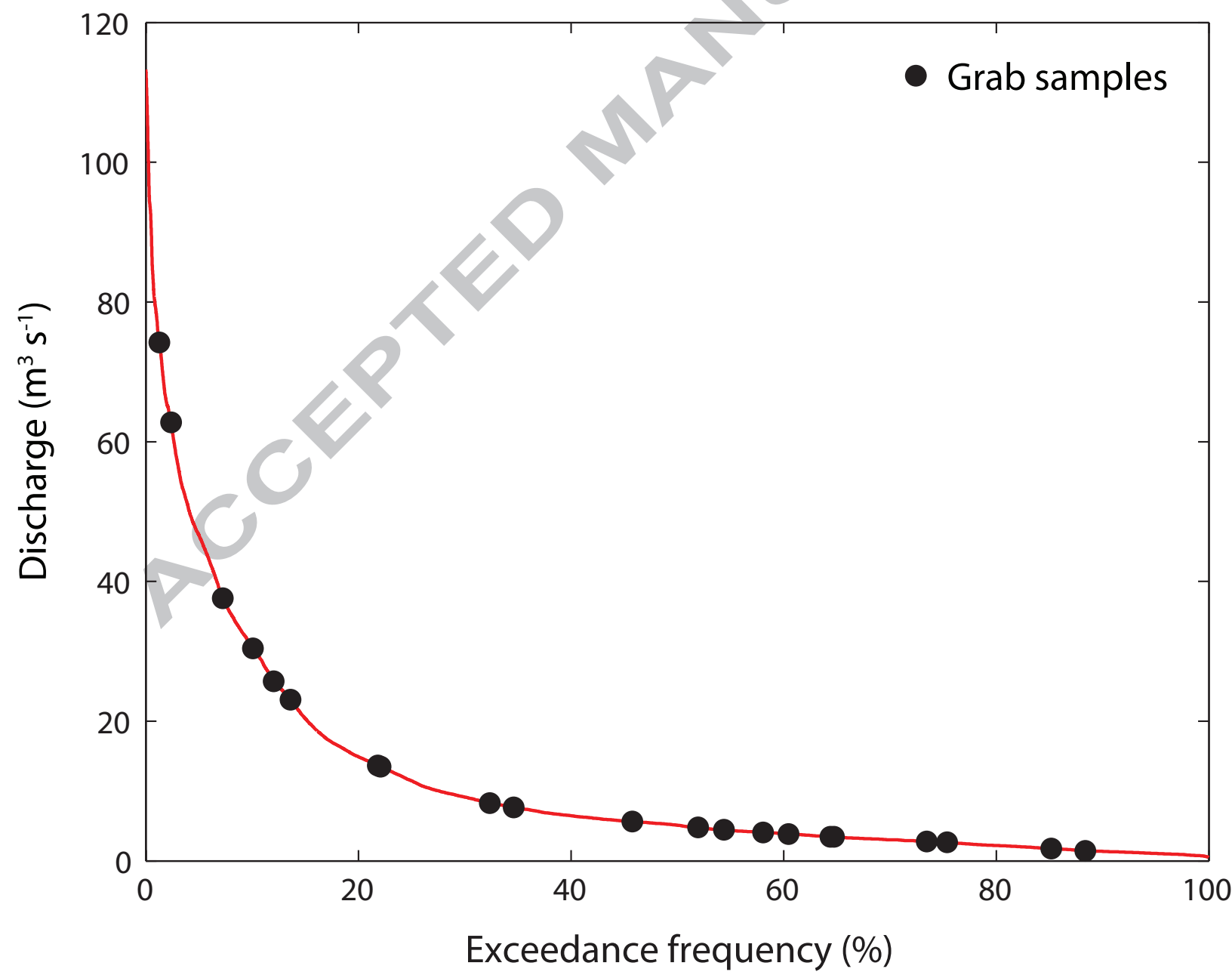


Figure3

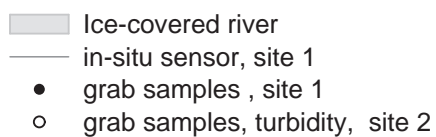
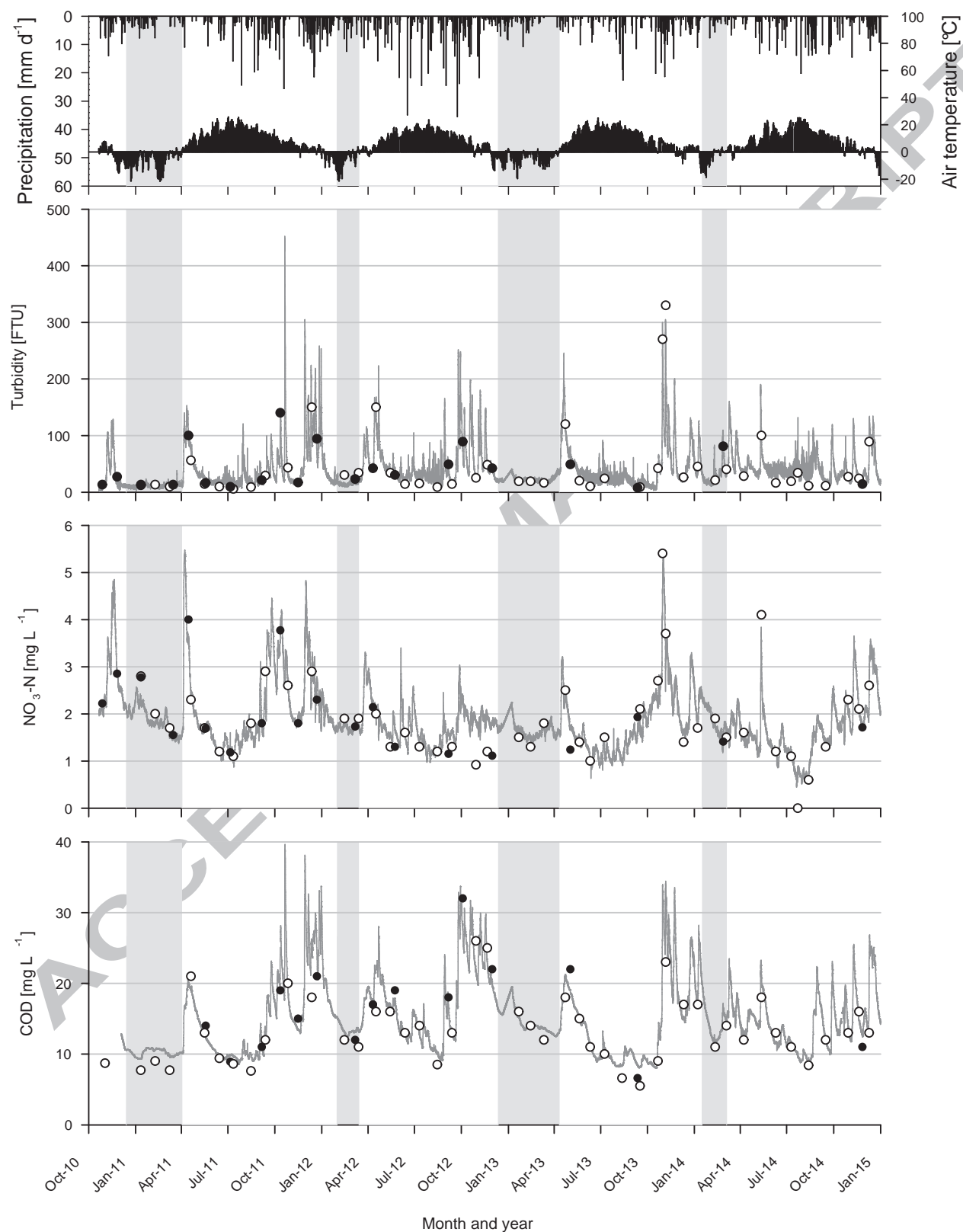


Figure4

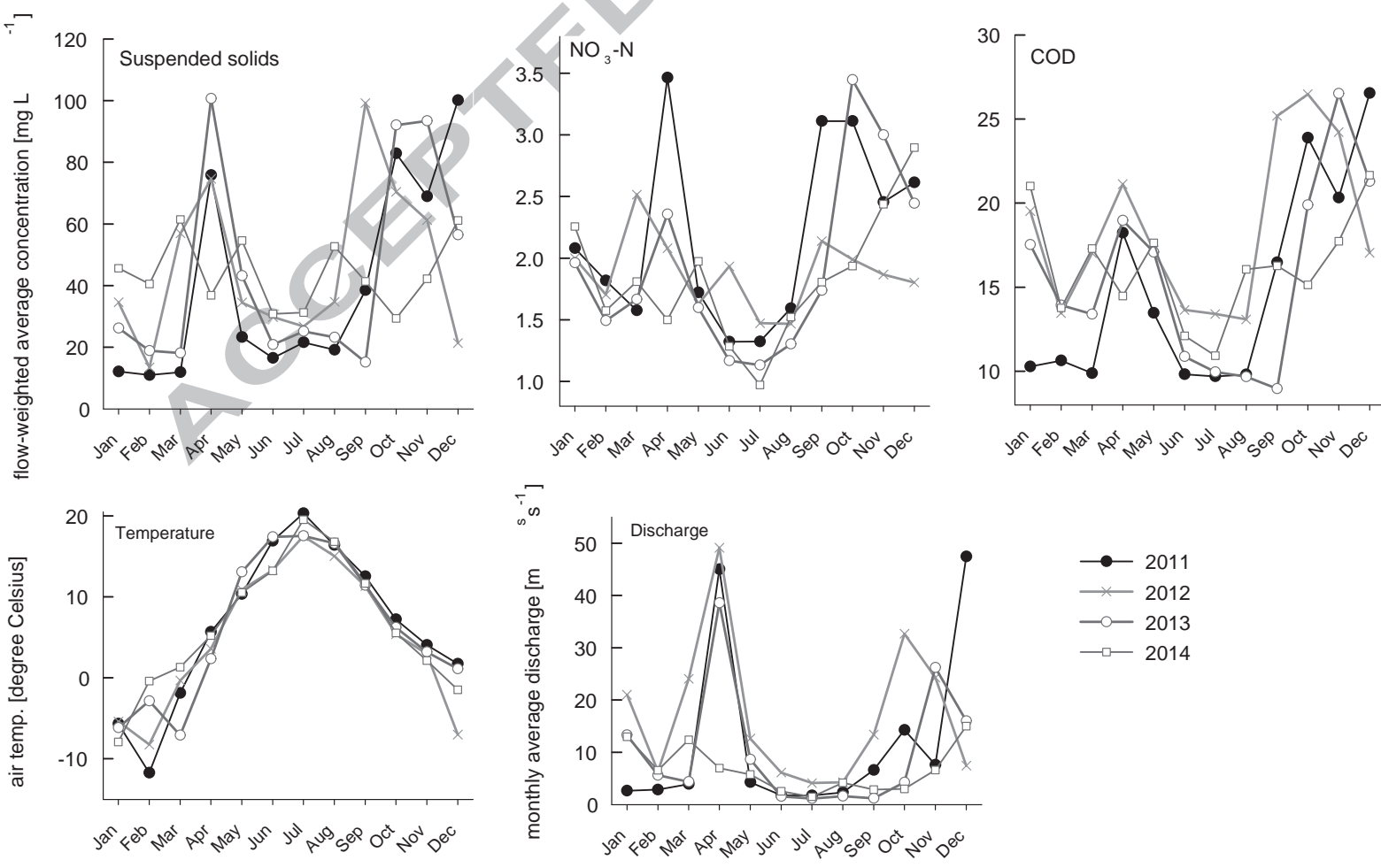


Figure5

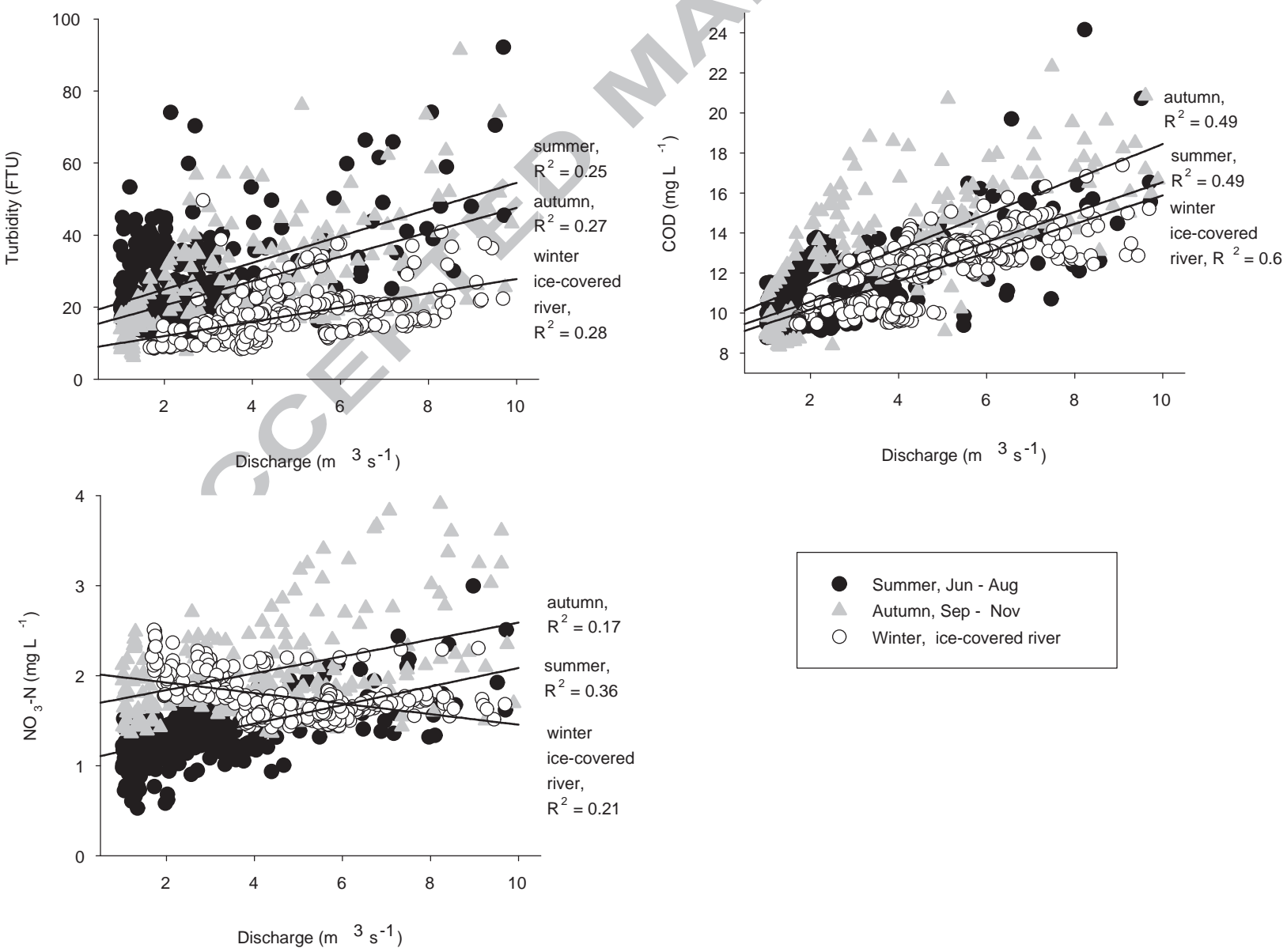
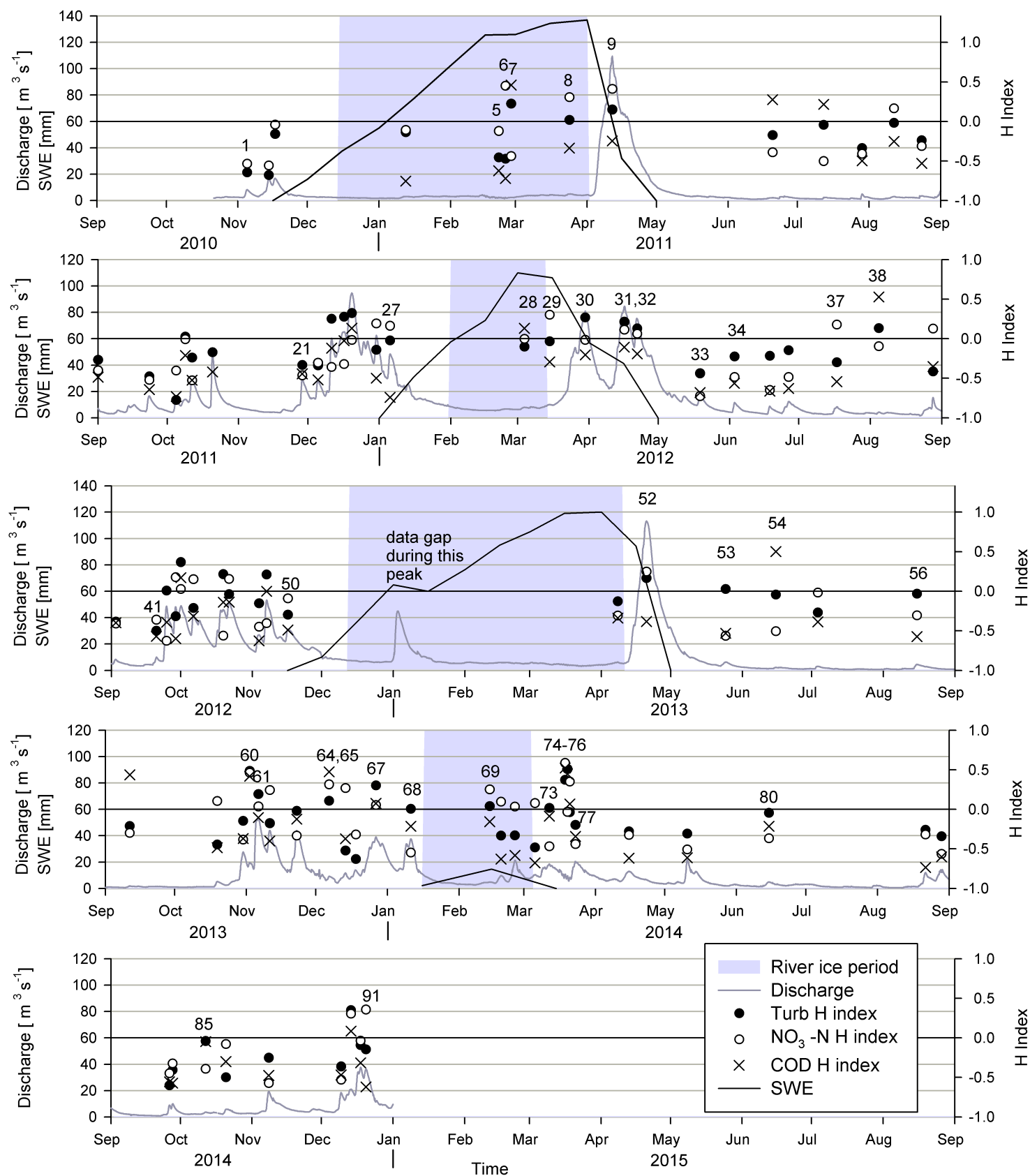


Figure6





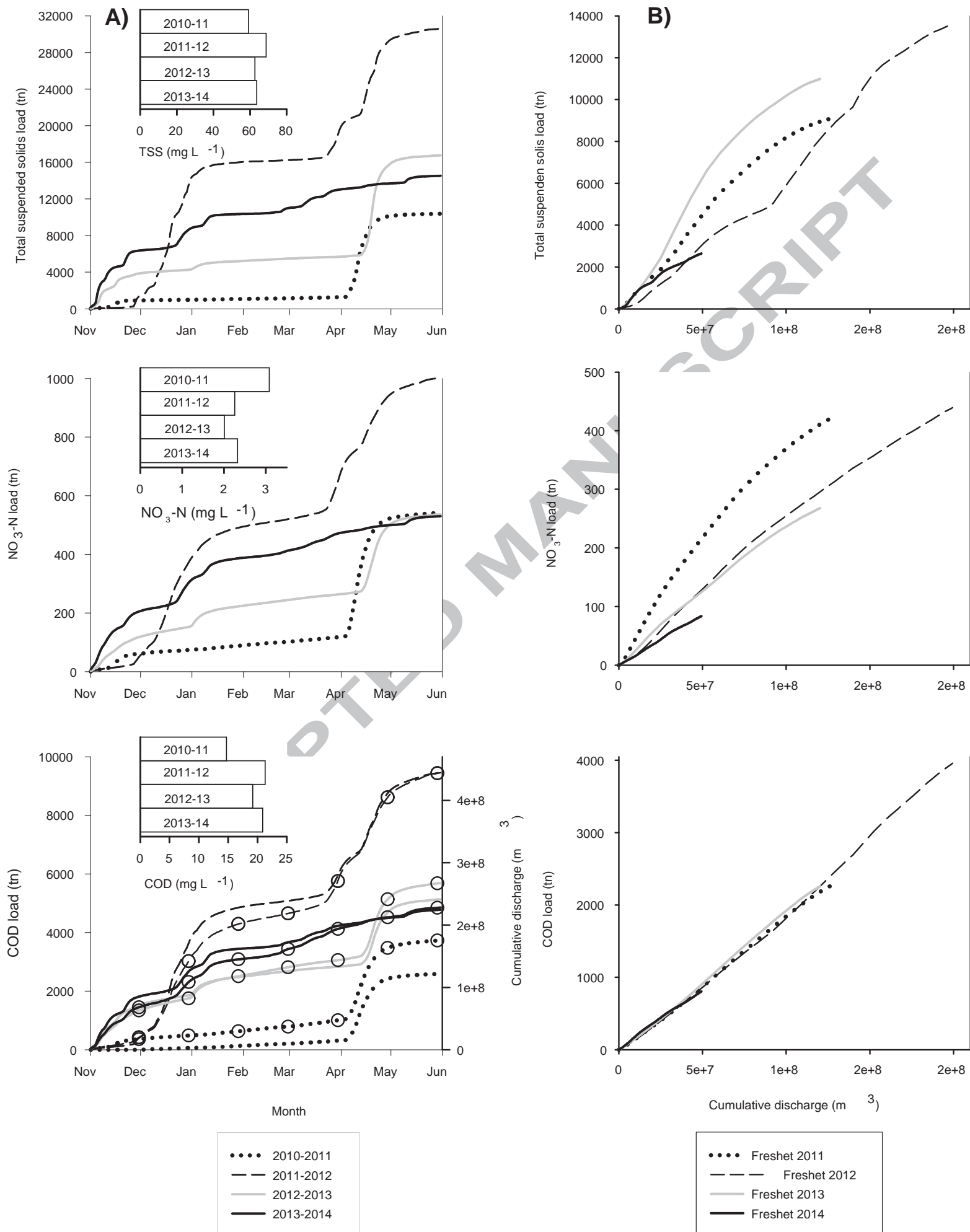


Figure8

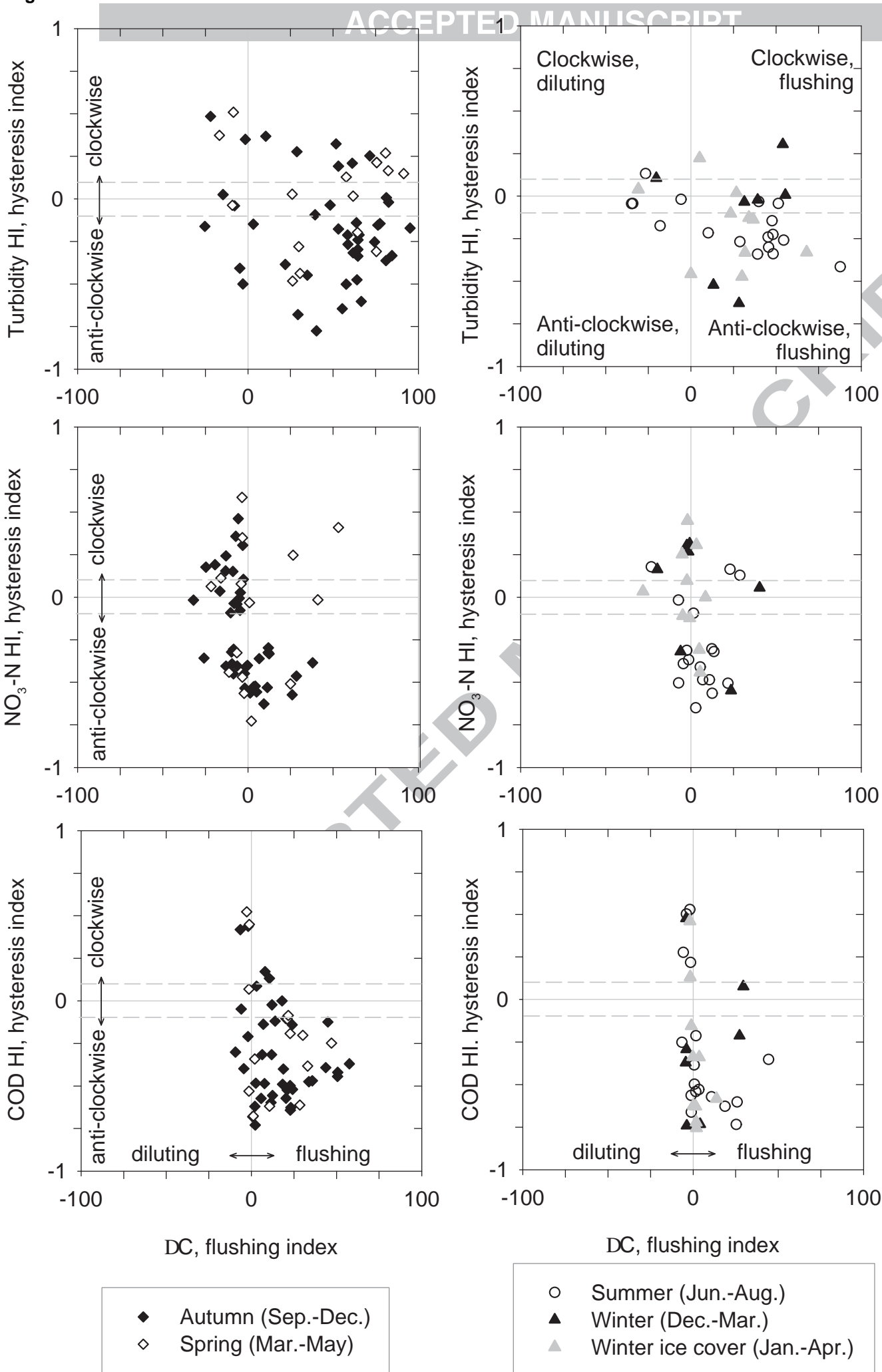
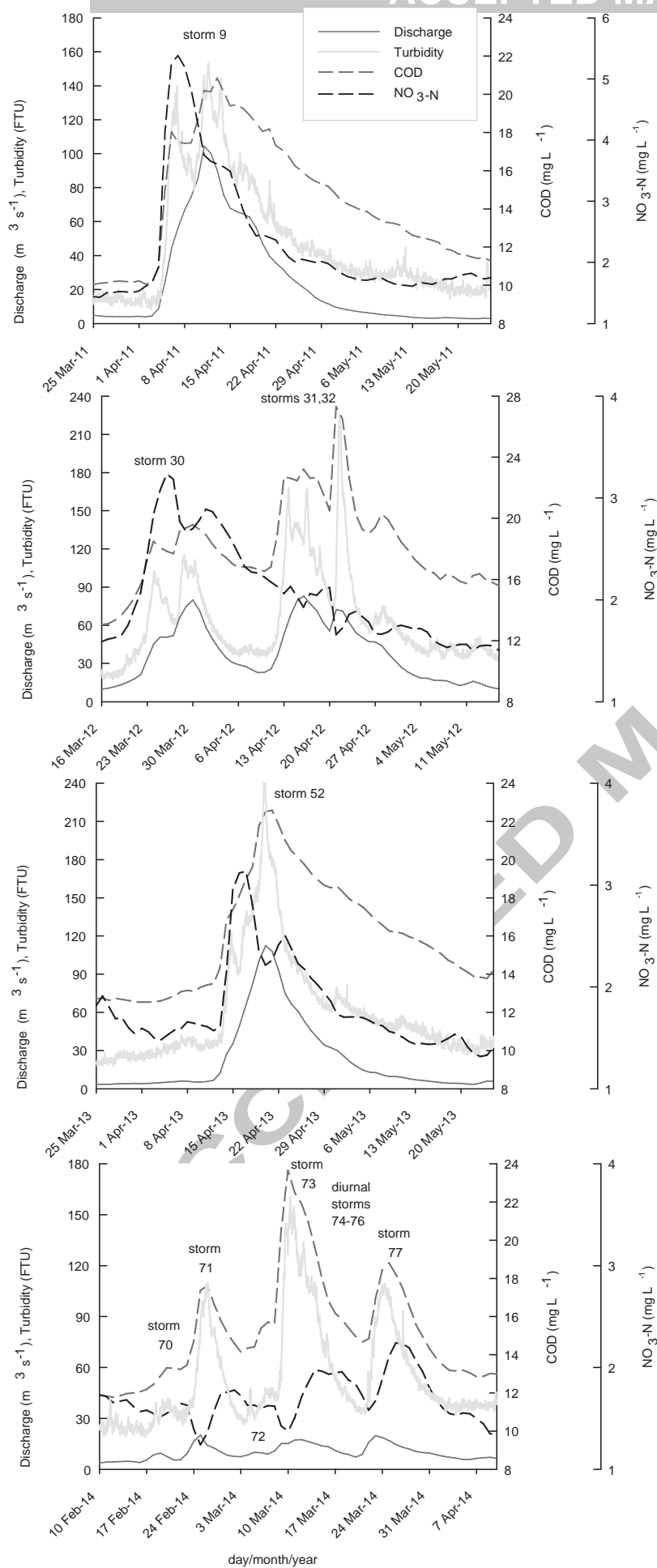
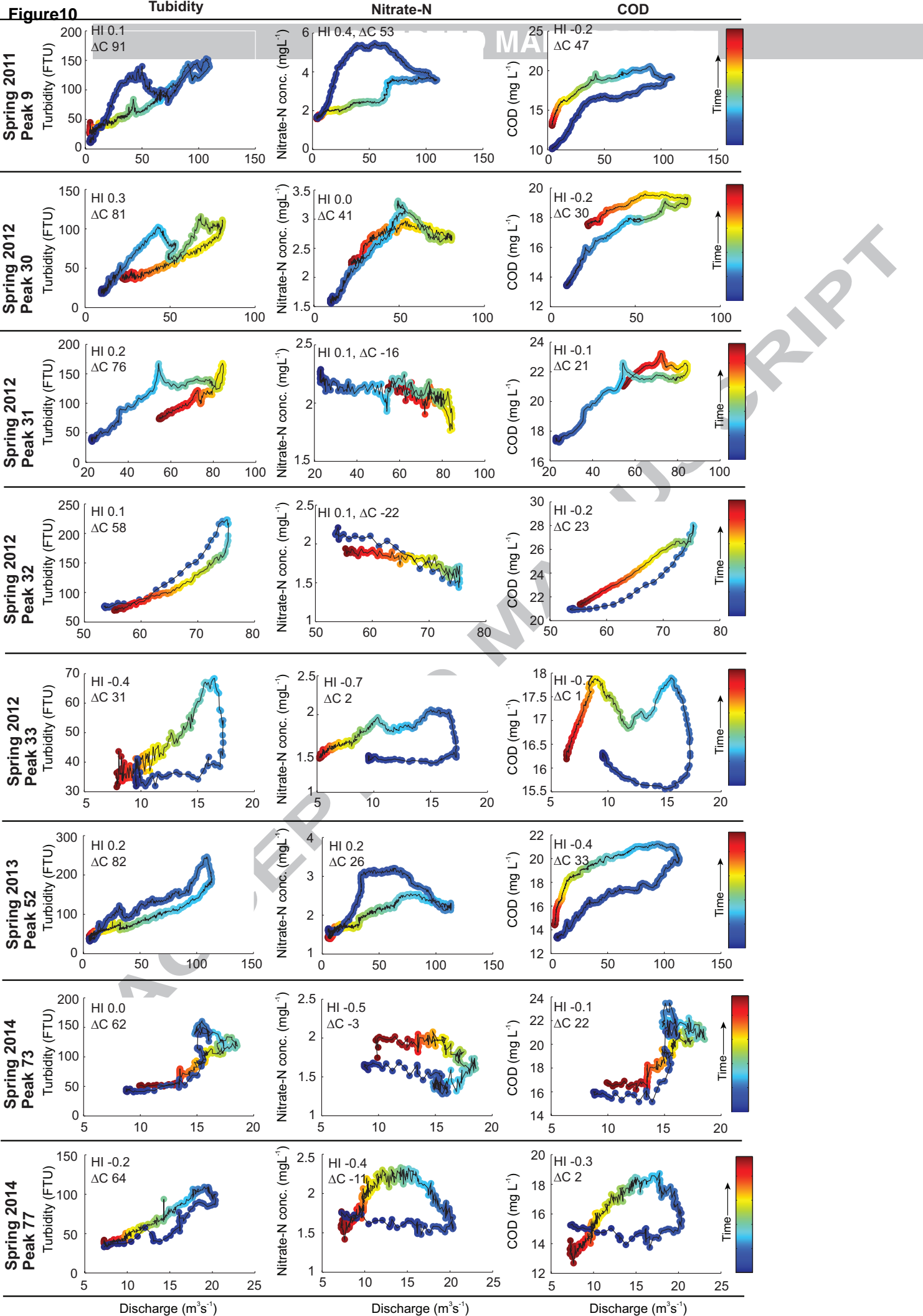


Figure9

ACCEPTED MANUSCRIPT





**Highlights:**

- River ice-cover decreases turbidity compared to summer or autumn baseflows
- Organic matter was flushing from the mixed land-use catchment during 91 storms
- Concentration peaks of turbidity, NO<sub>3</sub>-N and COD mainly lagged behind discharge peaks
- Overall turbidity peaks the fastest and NO<sub>3</sub>-N the slowest during the storms
- Snowpack and related unfrozen ground increased NO<sub>3</sub>-N availability for springtime flushing

Hysteresis of 3 water quality parameters during a snowmelt flow peak

